RIGA TECHNICAL UNIVERSITY

Oskars Platnieks

BIODEGRADABLE POLYBUTYLENE SUCCINATE WOOD PLASTIC COMPOSITES WITH ENHANCED EXPLOITATION PROPERTIES

Summary of the Doctoral Thesis

RTU Press
Riga 2022

RIGA TECHNICAL UNIVERSITY
Faculty of Materials Science and Applied Chemistry
Institute of Polymer Materials

Oskars Platnieks
Doctoral Student of the Study Programme "Materials Science"

BIODEGRADABLE POLYBUTYLENE SUCCINATE WOOD PLASTIC COMPOSITES WITH ENHANCED EXPLOITATION PROPERTIES

Summary of the Doctoral Thesis

Scientific supervisors
Professor Dr. sc. ing.
SERGEJS GAIDUKOVS
Professor Ph. D.
VIJAY KUMAR THAKUR

RTU Press
Riga 2022

Platnieks, O. Biodegradable Polybutylene Succinate Wood Plastic Composites with Enhanced Exploitation Properties. Summary of the Doctoral Thesis. – Riga: RTU Press, 2022.– 64 p.

Published in accordance with the decision of the Promotion Council "RTU P-02" of 24 March 2022, Minutes No. 04030-9.2.1/4.

Investigation, preparation, and testing of the materials was performed in the Institute of Polymer Materials of Riga Technical University.

This research was carried out within the scope of project WOODMIMIC, No. LZP-2018/1-0136, funded by the Latvian Council of Science.

https://doi.org/10.7250/9789934228155
ISBN 978-9934-22-815-5 (pdf)

ACKNOWLEDGEMENTS

I express my deepest gratitude to my wonderful family for their love, support, encouragement, and understanding.

I am extremely grateful to my supervisors Sergejs Gaidukovs and Vijay Kumar Thakur, for their guidance, support, motivation, and encouragement. I would like to extend my sincere thanks to colleagues and students for participating and contributing to this work. Thank you goes also to the reviewers for their constructive assessment, suggestions, and guidance.

I am obliged to the Institute of Polymer Materials of Riga Technical University and Latvian Council of Science for all the opportunities provided to me during my doctoral studies.

Perfection of character is this: to live each day as if it were your last, without frenzy, without apathy, without pretence.
/*Marcus Aurelius*/

DOCTORAL THESIS PROPOSED TO RIGA TECHNICAL UNIVERSITY FOR THE PROMOTION TO THE SCIENTIFIC DEGREE OF DOCTOR OF SCIENCE

To be granted the scientific degree of Doctor of Science (Ph. D.), the present Doctoral Thesis has been submitted for the defence at the open meeting of RTU Promotion Council on September 15, 2022 at 14.30 at the Faculty of Materials Science and Applied Chemistry of Riga Technical University, Paula Valdena iela 3/7, Room 272.

OFFICIAL REVIEWERS

Dr. sc. ing. Uģis Cābulis
Latvian State Institute of Wood Chemistry, Latvia

Professor Dr. Jordi Puiggalí
Universitat Politécnica de Catalunya, Spain

Professor Dr. Hom Dhakal
University of Portsmouth, United Kingdom

DECLARATION OF ACADEMIC INTEGRITY

I hereby declare that the Doctoral Thesis submitted for the review to Riga Technical University for the promotion to the scientific degree of Doctor of Science (Ph. D.) is my own. I confirm that this Doctoral Thesis had not been submitted to any other university for the promotion to a scientific degree.

Oskars Platnieks ……. (signature)
Date: ……

The Doctoral Thesis has been written in English and the total number of pages is 135. Summary of the Doctoral Thesis consists of an Introduction; Literature Review; Materials and Methods, Results and Discussion, Conclusions, 27 figures, 11 tables and the total number of pages is 64. The Bibliography contains 98 titles.

TABLE OF CONTENTS

ABBREVIATIONS

AFM	Atomic-Force Microscopy
APTES	3-Aminopropyltriethoxysilane
APTMS	3-Aminopropyltrimethoxysilane
CDI	Carbodiimide
CNC	Cellulose Nanocrystal
DMA	Dynamic Mechanical Analysis
DSC	Differential Scanning Calorimetry
EST	Aliphatic Ester
FTIR	Fourier Transform Infrared Spectroscopy
HDPE	High-Density Polyethylene
LDPE	Low-Density Polyethylene
MAH	Maleic Anhydride
MCC	Microcrystalline Cellulose
NFC	Nanofibrillated Cellulose
PBAT	Poly(Butylene Adipate Terephthalate)
PBS	Poly(Butylene Succinate)
PCL	Polycaprolactone
PE	Polyethylene
PET	Poly(Ethylene Terephthalate)
PHA	Polyhydroxyamide
PHB	Polyhydroxybutyrate
PLA	Poly(Lactic Acid)
PMDI	Polymeric Diphenylmethane Diisocyanate
PP	Polypropylene
rCell	Recycled Cellulose
SEM	Scanning Electron Microscopy
TGA	Thermogravimetric Analysis
wt.%	weight percent
WPC	Wood Plastic Composite

INTRODUCTION

Accumulation of commodity plastics pollution has become a significant challenge of the 21st century. Biodegradable and bio-based polymer materials have been developed to solve sustainability issues and preserve clean unpolluted environment. As these polymers become an inseparable part of the global market, more research is needed to produce composite materials with even higher properties to adapt to increasing demand from consumers. The potential to source plastics from renewable biomass and circular raw resources like forestry and agriculture waste, byproducts and even dedicated crops, has the potential to upset many industries. Some of the most promising applications are wood-plastic composites (WPCs), packaging, automotive, agricultural, and biomedical materials. The addition of cheap cellulose-based materials can lower the cost and improve physical and barrier properties and accelerate biodegradation. Contrary to popular belief, the plastics like poly(butylene succinate) (PBS) do not degrade in normal environment and use scenarios but require immersion in the soil and contact with microorganisms. Thus, the developed materials are up to industry standards and ready for upscaled production.

The development of PBS/cellulose composite materials from sustainable feedstock is demonstrated in the Doctoral Thesis. The use of recycled cellulose, microcellulose, and nanocellulose are explored in in-depth analysis outlining the prospects of every filler. In addition, chemical modification, compatibilization and surface coating methods are investigated. Recycled cellulose shows high potential for cheap and sustainable solutions. Processing the cellulose into nanosized particles shows exceptional properties that can be applied for advanced applications while retaining the biodegradability of PBS. The dynamical mechanical properties show that cellulose reinforcement extends to elevated temperatures, and materials retain the mechanical performance and do not become soft, like neat polymer. The extensive range of studied filler loadings allows to select the optimized performance of the composites.

Within the scope of the Doctoral Thesis, the PBS/nanocellulose composite preparation method was optimized using a highly loaded masterbatch process to reduce the use of organic solvents. Masterbatch process is compatible and scalable with industrial production methods like extrusion and injection moulding. It was concluded that the process is more efficient and yields higher mechanical properties due to to high shear mixing, promoting excellent dispersion.

The biodegradation was extensively studied in composting conditions. All tested samples disintegrated in the soil within 3 months. Calorimetry and infrared spectroscopy confirmed the biodegradation process of the prepared composite materials. The water immersion was studied at room temperature to confirm the excellent dimensional stability of tested samples. While the quality of prepared materials was checked using the fracture surface produced in liquid nitrogen and examined in scanning electron microscopy.

Aim of the Doctoral Thesis

The aim is to develop biodegradable poly(butylene succinate)/cellulose composite materials with enhanced exploitation properties using sustainable resources and technologies.

Tasks of the Doctoral Thesis

1. To obtain woody-like sustainable polymer composite materials from recycled cellulose powder, microcellulose, nanocellulose, and biobased poly(butylene succinate) polymer.
2. To compare microcellulose and nanocellulose composites obtained by solution and melt blending processing technology.
3. To investigate the obtained cellulose composites' tensile, thermomechanical, thermal, and biodegradation properties.
4. To assess different modification and compatibilization methods for cellulose composites.
5. To enhance the exploitation properties of the cellulose composite materials.

Thesis statements to be defended

1. High-loading sustainable PBS/cellulose composites can be prepared by solution, melt, and masterbatch processes.
2. The masterbatch preparation is a more sustainable route for producing PBS/nanocellulose composites compared to the solution and direct melt mixing processes.
3. Chemical modification of the cellulose can significantly enhance the exploitation (thermal, tensile, thermomechanical) properties of PBS composite materials.
4. Biodegradation of PBS/cellulose composites can be controlled by the cellulose type, the chemical modification route, and the cellulose filler content.

Scientific novelty

1. Demonstration of sustainable, biodegradable composites as an alternative to fossil-based plastics for high-performance applications.
2. The proposed chemical modification routes of cellulose can adjust the exploitation properties of the PBS/cellulose composite materials.
3. The solution, melt, and masterbatch processes were developed to produce PBS/cellulose composites.

Practical significance

1. Developed sustainable poly(butylene succinate)/cellulose composite materials can be applied for biodegradable food packaging, cutlery, decks, mulch films, and many

sustainable products to replace fossil non-biodegradable polyolefins and wood-plastic composites.
2. The developed PBS/cellulose masterbatch process and cellulose modification protocols can upscale the production of these composite materials.
3. Paper, cardboard, and agricultural waste can be a sustainable source of cellulose for PBS composite preparation.

Approbation of the Thesis in Scopus and Web of Science indexed articles

Literature Review

1. **O. Platnieks**, S. Gaidukovs, V. K. Thakur, A. Barkane, S. Beluns. Bio-based poly (butylene succinate): Recent progress, challenges and future opportunities. European Polymer Journal, 161, (2021), 110855, doi:10.1016/j.eurpolymj.2021.110855.
   Chapter 3.1.
2. **O. Platnieks**, A. Barkane, N. Ijudina, G. Gaidukova, V. K. Thakur, S. Gaidukovs. Sustainable tetra pak recycled cellulose / Poly(Butylene succinate) based woody-like composites for a circular economy. Journal of Cleaner Production, 270, (2020), 122321, doi:10.1016/j.jclepro.2020.122321.
   Chapter 3.2.
3. **O. Platnieks**, S. Gaidukovs, A. Barkane, A, Sereda, G. Gaidukova, L. Grase, V. K. Thakur, I. Filipova, V. Fridrihsone, M. Skute, M. Laka. Bio-based poly(butylene succinate)/microcrystalline cellulose/nanofibrillated cellulose-based sustainable polymer composites: Thermo-mechanical and biodegradation studies. Polymers, 12(7), (2020), 1472, doi:10.3390/polym12071472.
   Chapter 3.3.
4. **O. Platnieks**, A. Sereda, S. Gaidukovs, V. K. Thakur, A. Barkane, G. Gaidukova, I. Filipova, A. Ogurcovs, V. Fridrihsone. Adding value to poly (butylene succinate) and nanofibrillated cellulose-based sustainable nanocomposites by applying masterbatch process. Industrial Crops and Products, 169, (2021), 113669, doi:10.1016/j.indcrop.2021.113669.
   Chapter 3.4.
5. **O. Platnieks**, S. Gaidukovs, A. Barkane, G. Gaidukova, L. Grase, V. K. Thakur, I. Filipova, V. Fridrihsone, M. Skute, M. Laka. Highly loaded cellulose/poly (butylene succinate) sustainable composites for woody-like advanced materials application. Molecules, 25(1), (2020), 121, doi:10.3390/molecules25010121.
6. S. Gaidukovs, **O. Platnieks**, G. Gaidukova, G. O. Starkova, A. Barkane, S. Beluns, V. K. Thakur. Understanding the Impact of Microcrystalline Cellulose Modification on Durability and Biodegradation of Highly Loaded Biocomposites for Woody Like Materials Applications. Journal of Polymers and the Environment, 30(4), (2022), 1435–1450, doi:10.1007/s10924-021-02291-3.

Other publications on the topic that are not included in the Thesis

1. N. Neibolts, **O. Platnieks**, S. Gaidukovs, A. Barkane, V. K. Thakur, I. Filipova, G. Mihai, Z. Zelca, K. Yamaguchi, M. Enachescud. Needle-free electrospinning of nanofibrillated cellulose and graphene nanoplatelets based sustainable poly (butylene succinate) nanofibers. Materials Today Chemistry, 17, (2020), 100301, doi: 10.1016/j.mtchem.2020.100301.
2. **O. Platnieks**, S. Gaidukovs, N. Neibolts, A. Barkane, G. Gaidukova, V. K. Thakur.Poly(butylene succinate) and graphene nanoplatelet–based sustainable functional nanocomposite materials: structure-properties relationship. Materials Today Chemistry, 18, (2020), 10035, doi: 10.1016/j.mtchem.2020.100351.
3. G. Gaidukova, **O. Platnieks**, A. Aunins, A. Barkane, C. Ingrao, S. Gaidukovs. Spent coffee waste as a renewable source for the production of sustainable poly(butylene succinate) biocomposites from a circular economy perspective. RSC Advances, 11(30), (2021), 18580–18589, doi: 10.1039/D1RA03203H.

Dissemination in international scientific conferences

1. **O. Platnieks**, S. Gaidukovs, N. Ijudina. Use of recycled cellulose filler from Tetra Pak® packaging waste for melt processing by kinetic mixer of polybutylene succinate based composites. *Baltic Polymer Symposium 2018*, Jurmala, Latvia, September 12–14.
2. **O. Platnieks**, S. Gaidukovs, N. Ijudina. Polybutylene Succinate and Recycled Cellulose Filler Composites. *Materials Science and Applied Chemistry, 2018*, Riga, Latvia, October 26.
3. **O. Platnieks**, S. Gaidukovs, V. K. Thakur, I. Filipova. Sustainable Graphene, Nanocellulose and Bio-based Polybutylene Succinate Composites. *Graphene Week, 2018*, Donostia/San Sebastian, Spain, September 10–14.
4. **O. Platnieks**, N. Neibolts, S. Gaidukovs, A. Barkane, V. K. Thakur, I. Filipova, V. Fridrihsone, M. Enachescu, Z. Zelca. Characterization of electrospun nanofibers of poly(butylene succinate) blends with nanofibrillated cellulose. *Baltic Polymer Symposium, 2019*, Vilnius, Lithuania, September 18–20.
5. **O. Platnieks**, A. Barkane, V.K. Thakur, I. Filipova, V. Fridrihsone, S. Gaidukovs. Wood-like biobased and biodegradable polybutylene succinate microcellulose composites. *The Conference on Green Chemistry and Nanotechnologies in Polymeric Materials 2019*, Riga, Latvia, October 9–11.
6. **O. Platnieks**, N. Neibolts, S.Gaidukovs, V. K. Thakur, I. Filipova. Polybutylene Succinate/Cellulose/Graphene Composites. *Materials Science and Applied Chemistry, 2019*, Riga, Latvia, October 24.
7. **O. Platnieks**, S. Gaidukovs. Nanofibrillated cellulose modification methods for potential polymer-based aerogel fabrication. *International Conference on Aerogels for Biomedical and Environmental Applications, 2020*, Santiago de Compostela, Spain, February 18–20.

8. **O. Platnieks**, A. Sereda, S. Gaidukovs. Enhanced dispersion of nanofibrillated cellulose in poly (butylene succinate) matrix via combination of solvent casting and melt blending for functional green nanocomposites. *1st International Greenering conference*, Costa da Caparica, Portugal, February 15–16, 2021.

1. SUMMARY OF LITERATURE REVIEW

PBS has often been compared to PE and presented as a biodegradable alternative. PBS is soft and flexible semi-crystalline polyester with melting temperature around 110 °C to 115 °C and heat deflection temperature of 95 °C. In comparison, commercial variations with additives or copolymers can be with significantly lower temperatures. The disparity between reported properties comes from confusing the PBS copolymers with PBS due to manufacturer marketing and various modifications, like chain extension playing a significant role in PBS properties. M_w bellow 1×10^5 g/mol is considered a low-quality polymer which is more brittle, while higher molecular weight yields good PBS with excellent properties suitable for extrusion, film blowing and injection molding [1]. Xu et al. reported that PBS reaches suitable properties for film blowing when M_w is around 1.8×10^5 g/mol [1].

Excellent mechanical properties of high molecular weight combined with thermal stability, high heat deflection temperature, and good processability suitable with conventional methods have resulted in PBS being seen as a commercial biodegradable alternative to polyethylene (PE) and polypropylene (PP). PBS is safe in contact with food, which significantly expands applications in the food industry, while heat deflection enables contact with hot beverages [2]. Higher density of PBS can be seen as a drawback; lower melting temperature results in reduced energy requirements for material melt-processing.

Globally, bio-based plastics production has exceeded 2 million tons, with an expected 3 million tons by 2024 [3]. Overall, they contribute less than 1 % of annual plastic production, exceeding 400 million tons [4]. Around 55 % of bio-based plastics are biodegradable, of which most notable are PLA, PBAT, PBS, PCL, PHA, and biodegradable starch blends [3]. Commercial production of PBS was pioneered by Showa Denko (Japan) under brand name Bionolle™ produced from 1993 till 2016 when the production was stopped by the company, citing delay in permeation of environmental regulations on plastic shopping bags [5]. Mitsubishi Chemical Corporation (Japan) in 2003 started the PBS production under brand name GS Pla™ which was produced from fossil sources, while in 2015, a commercial production plant producing bio-based (50 %) PBS was opened in Thailand in partnership with PTT Public Company Limited (Thailand) using brand name BioPBS™ [6], [7]. In the last decade, PBS production plants were built in China (Hexing Chemical and Xinfu Pharmaceutical) and Korea (Ire Chemical and SK Polymers) [7], [8]. With the introduction of new technologies, the production of fully bio-based PBS is estimated to have at least 15–20 % lower impact on the environment compared to petrochemical incumbents when the cradle-to-grave system was examined [9].

Bacteria and fungi can degrade aliphatic polyesters, including PBS. Manufacturers recommend using composting conditions with a temperature above 30 °C, while studies on PBS biodegradation often use around 58 to 65 °C combined with high water content in the soil [10]. Kim et al. reported that PBS biodegradation in natural soil at temperature 60 °C resulted in around 10 wt.% mass loss over 120 days [11]. A study using compost soil with 30 °C temperature reported around 30 wt.% loss in 180 days, and the authors also noted that addition of jute fibers significantly accelerated degradation [12]. While the combination of composting

soil and 58 °C resulted in total degradation of PBS in around 100 days [13]. This was confirmed by the analysis of evolved carbon dioxide. Similar results with composting conditions and 58 °C were reported by other authors [14]. Cho et al. studied PBS degradation in landfills and concluded that PBS degradation was relatively slow, but pretreatment methods like thermal, enzymatic, ultrasonic treatment and the application of adapted microorganisms significantly enhanced the decomposition speed [15]. It has been reported that PBS degrades in the marine environment; indeed, exceptional property to reduce sea pollution [10]. Unfortunately, PBS degradation was estimated to relatively slow around 2 wt.% for a time of 2 to 3 months in the reported studies [16], [17].

PBS comes with crucial properties such as good mechanical performance, high ductility and elongation at a break that can exceed 200 %, good thermal stability and processability, including, chemical resistance [18], [19]. The combination of these properties makes PBS especially attractive for polymer composite preparation [20]–[22]. The addition of filler material can selectively increase gas barrier properties, yield higher stiffness, and even reduce the material costs [23]. In addition, abundance, renewability, biodegradability, and low density have played a significant role in organic filler popularity [24]. Mochane et al. reported that PBS/natural fiber composites offer significant advantages like reducing the emission of pollutants, increasing energy recovery and biodegradability [25]. The authors outlined substantial disadvantages of the high flammability of such composites. Xiao et al. reviewed developments in fire retardancy of PBS [26]. The authors summarized that several approaches exist to improve fire retardancy, like inorganic fillers magnesium hydroxide, expanded graphite, carbon black, and organic lignin. In addition, a promising combination of ammonium polyphosphate and melamine has gained a lot of interest [26]. Most of these additives do not significantly hinder applications, as they have almost no toxicity or impact on biodegradability.

Short-term use of light packaging materials and films is problematic for recovery and recycling of plastics [27]. These products often end up in landfill, soil, forest, or ocean contributing to major pollution, which can be avoided with use of bioplastics. The remains of plastics in soil can significantly reduce yield of crops and contribute to food supply issues in long term [28]. Once microplastics are formed, it is almost impossible to collect them from soil or water, but they will remain in this form for hundreds of years. While their impact on humans and animals is only being studied, the alarming rate of their rising content in nature has pushed for new policies and legislations [29].

New applications of bioplastics are introduced every year resulting in a growing market size. Since the PBS biodegradation has been widely studied and it degrades into water and carbon dioxide, it is presented as an alternative to commodity polymers like PET, PP, LDPE, HDPE [2], [30], [31]. The manufactures and scientists alike have presented these comparisons, which show a great feasibility for replacement of commodity plastics owing to similar thermal and mechanical properties [30]–[32]. Manufacturers like Mitsubishi Chemicals have suggested application mainly in food packaging and agriculture industries [32]. In addition, there is great potential for biomedical applications, like scaffolds for tissue recovery, drug delivery and implants [21], [33], [34]. While large industries, like automotive, are pushing for sustainable manufacturing [35].

2. MATERIALS AND METHODS

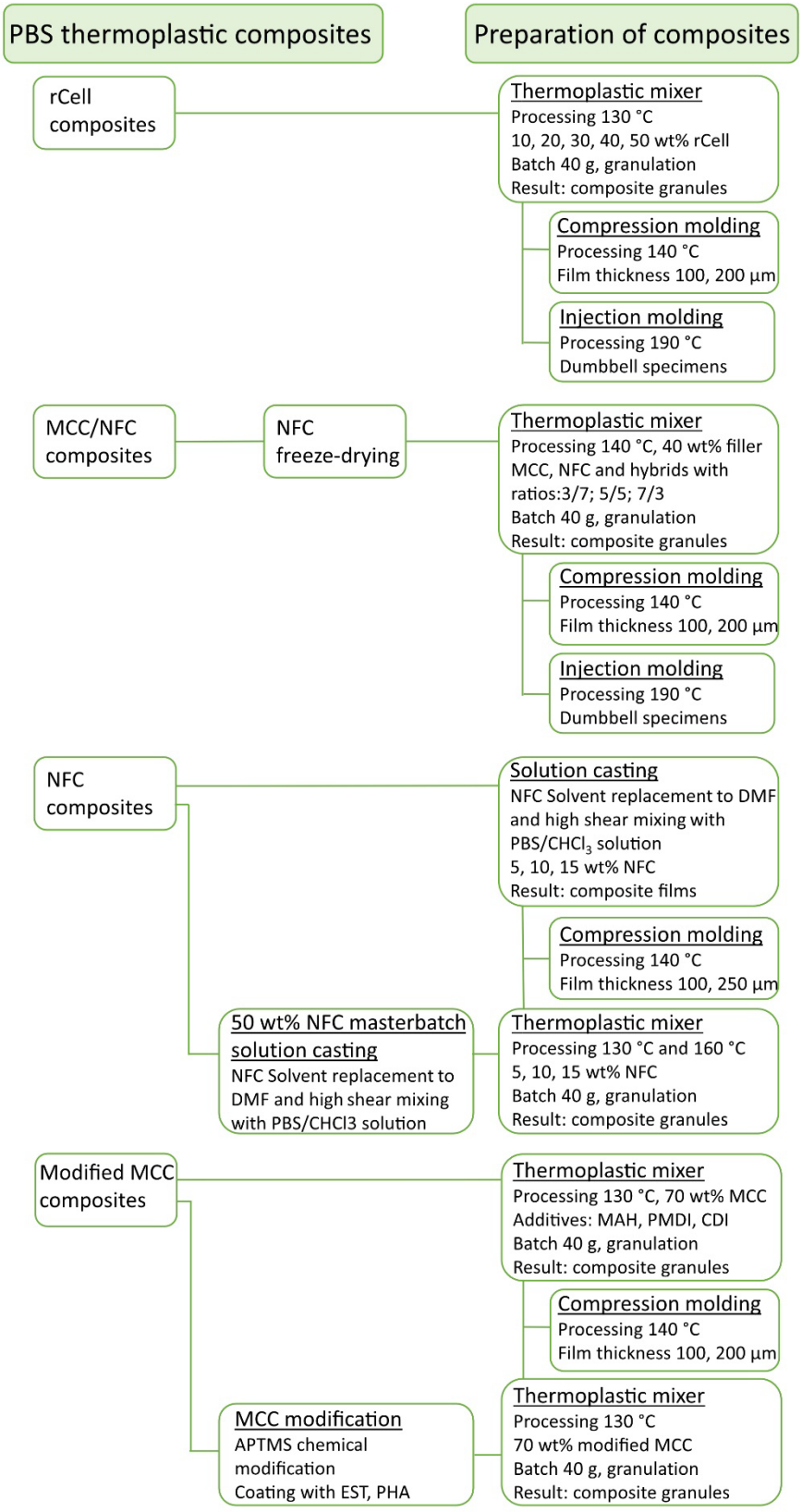

Fig. 2.1. Structure of the research.

2.1. Materials

Polymer

The selected Polybutylene succinate (PBS) was BioPBS™ grade FZ71PB® (PTT MCC Biochem Company Ltd) and, which, according to the producer, was bio-based (50 wt.%), biodegradable thermoplastic polymer [2]. The bio-based content comes from bio-succinic acid used in the synthesis. Its inherent melting point is 115 °C, density − 1.26 g/cm^3, and melt flow index − 22 g / 10 min (2.16 kg, 190 °C). According to the manufacturer, FZ71 is flexible semi-crystalline polyester with excellent properties suitable for cast extrusion and extrusion coating. It can be used in contact with food and hot beverages with temperatures up to 100 °C. In addition, PBS is compostable in soil, landfills and at home, while the recommended temperature for compost is at least 30 °C.

Recycled cellulose

The rCell was received from the TetraPak® recycling industry company as a recycled cellulose pulp that was separated from aluminium and polymer components during industrial-technological processing. Before laboratory processing the pulp was ground with the Retsch cutting mill SM300. A 4 mm sieve was used followed by the second milling with a sieve size of 250 μm. The mill was fed manually, and the rotation speed was set for the whole process at 1500 rpm. rCell is a fibre filler, characterized by average length of 200 μm and average width − 20 μm.

Microcrystalline cellulose

Microcrystalline cellulose was obtained from bleached softwood kraft pulp (Metsä Botnia AB) according to the procedure reported by the authors [76]. In compliance with this method, the pulp was impregnated with a thermocatalytic degradation catalyst – weak hydrochloric acid solution (0.05 %); the used modulus was 1:20. After pressing out the excess liquid, the pulp was thermally treated at a temperature of 120 ºC until a dry state. This facilitated the destruction of the amorphous part of cellulose, while the crystalline part remained almost intact. The degree of polymerization decreased and reached the so-called levelling-off degree of polymerization (LODP), which, in the case of cellulose, was ~250 units [77]. Then, the partially degraded pulp was ground in a ball mill "U.S. Stoneware JAR MILL 755RMV1" (USA) with variable speed. The milling jar was made from alumina-fortified porcelain, with a capacity of 5.7 L. Cylindrical grinding media from corundum 2.1cm x 2.1cm in size were used; charging factor was 1 kg/L and grinding time ~15 h. As a result, microcrystalline cellulose powder was obtained. Average size of obtained MCC particles was 10–40 μm obtained from SEM. Zeta potential for the obtained MCC particles was about –16.9 mV.

Nanofibrillated Cellulose

Nanofibrillated cellulose gel-like dispersion (11 wt.%) was prepared using mechanical treatment with the previously established thermo-catalytic method. NFC fabrication is like MCC preparation but involves the addition of water after the drying process and wet milling (instead of dry milling for MCC) of the cellulose for 15 h. The length of NFC was measured in a range from 200 to 550 nm with an average of 350 nm by dynamic light scattering (Malvern

Nano ZS-90) and the diameter was obtained from AFM with size distribution between 15–50 nm.

Other chemicals

Laboratory grade hydrochloric acid, chloroform and N,N-dimethylformamide (DMF) were purchased from Merck KGaA (Darmstadt, Germany). Carbodilite® HMV-15CA was purchased from Nisshinbo Chemical Inc (Japan). Carbodilite contained a carbodiimide (CDI) group, which worked as a chain extender and hydrolysis stabilizer. Addapt® BioWet 25 L is a solvent-free water-based, readily biodegradable surfactant based on polyhydroxy amides (PHA). Addapt® Ester 80DA is a water and solvent-soluble synthetic aliphatic ester (EST) dispersing agent. BioWet 25 L and Ester 80DA were both purchased from Adapt Chemicals B.V (Netherlands). 3-Aminopropyltrimethoxysilane (APTMS), maleic acid anhydride (MAH), and acetic acid were purchased from Sigma–Aldrich (Germany). Polymeric diphenylmethane diisocyanate IsoPMDI 92140 (PMDI) was purchased from BASF (Germany).

2.2. Testing Methods

Dynamic light scattering

Zeta potential and size of particles for MCC were determined on Zeta Sizer Nano ZS90 (Malvern, UK) for 0.05 wt.% suspension in distilled water.

Optical microscopy

The rCell particle sizes were calculated from the images of particles deposited on the glass slide, which were taken using an optical microscope Leica DMR (Leica Microsystems, Germany) at 5x, 10x magnifications. Leica Image Suite™ software was applied for particles' length and width measurements.

Differential scanning calorimetry

The Mettler DSC-1 instrument was used for calorimetric tests. Samples with a weight around 10 mg were scanned in heating and cooling modes from 30 to 150 °C in a nitrogen atmosphere. The heating and cooling rate was set to 10 °C /min, and the specimens were kept at a constant temperature for 5 min before cooling and second heating. The crystallization and melting temperatures, enthalpies, and crystallinities, respectively, were calculated from the experimental heating and cooling curves. The melting peak crystallinity of the PBS and the composites was calculated using the following equation:

$$\chi_m = \frac{\Delta H_m}{\Delta H_m^o (1-W_{Cel})} \times 100\% , \qquad (1)$$

where ΔH_m corresponds to the measured melting crystallization enthalpy of the specimen, ΔH_m^o is the theoretical melting enthalpy of 100 % crystalline polymer (110.5 J/g for PBS [36]), and W_{Cel} is the cellulose filler weight fraction in the composition.

The crystallization peak crystallinity of the PBS and the composites was calculated using the following equation:

$$\chi_c = \frac{\Delta H_c}{\Delta H_m^o (1-W_{Cel})} \times 100\% , \qquad (2)$$

where ΔH_c corresponds to the measured cooling peak crystallization enthalpy of the specimen.

Thermogravimetric analysis

The thermogravimetric tests were performed on a Mettler TG50 instrument. Specimens about 10 mg in weight were heated in the air up to 800 °C. The thermal stability of material was evaluated from the weight-loss heating curves. The weight loss was calculated according to ASTM D3850 using the Mettler original software.

Hydrostatic density testing

Density d was determined by weighing the material in air and ethanol on Sartorius KB BA 100 electronic scales equipped with a Sartorius YDK 01 hydrostatic density measurement kit. The density of the PBS and the composites was calculated using the following equation:

$$d_p = \frac{m_a(d_{EtOH} - 0.00120)}{0.99983(m_a - m_s)} + 0.00120\,, \qquad (3)$$

where m_a is the sample's measured mass in air atmosphere, m_s is the sample's measured mass when the sample is submerged in ethanol, and d_{EtOH} is the density of ethanol, which was measured with the aerometer.

The theoretical density of the composites was calculated using the following equation:

$$d_t = d_{Cel}\varphi_{Cel} + d_{PBS}(1 - \varphi_{Cel}), \qquad (4)$$

where d_{Cel} is the density of cellulose 1.50 g cm^{-3} (obtained from the literature [37]), ϕ_{Cel} is the volume fraction of cellulose in the composite, and d_{PBS} is the experimental density of PBS. At least 10 parallel samples were tested.

Vickers microhardness

The Vickers microhardness was measured on a Vickers M-17 1021 device equipped with an optical microscope lens magnification 4 times with a 0.20 kg load and a loading time of 20 s.

The Vickers microhardness of the PBS and the composites was calculated using the following equation:

$$H_V = \sin\left(\frac{\alpha}{2}\right)\frac{P \cdot g}{(d \cdot k \cdot n/1000)^2}\,, \qquad (5)$$

where α is the diamond pyramid facet angle (136° from the specification of the instrument), P is the applied load, g is the standard acceleration due to gravity (9.807 m/s^2 was used), d is the average diagonal value of pyramid's indentation, k is the correction factor for the applied load (1.00 from the specification of the instrument for 0.20 kg load), and n is the correction factor for lens magnification used (1.30 from the specification of the instrument for 4 times magnification).

Fourier transform infrared spectroscopy performed in attenuated total reflectance mode

The FTIR was used to study the bonding and interactions between the components of the prepared PBS/rCell composites. FTIR spectra of composites were collected at a resolution of 4 cm^{-1} on a Nicolet 6700 (ThermoScientific, Germany) in the region of 800–4000 cm^{-1}. Sixteen measurements of every specimen were performed, and the average spectrum is shown; the measurement error was 1 %.

Dynamic mechanical analysis

The force and displacement amplitudes and phase shifts were determined with the dynamic mechanical analyser Mettler DMA/SDTA861e. The specimens were tested at a temperature interval –80...+80 °C, the applied force was 5N, elongation – 10μm, frequency – 1 Hz and

heating rate – 3 deg/min in tension mode. The tested specimens were 8.50 mm long, 4.00 mm wide, and 0.15 mm thick, preconditioned in 50 % relative humidity at room temperature for 24 h.

Scanning electron microscopy

The morphology of dispersion in the polymer matrix was analysed with Phenom Desktop SEM (USA) for the results section (Section 3.1). The images were obtained using a 10 kV voltage setting. The surfaces of the PBS/rCell samples used for the measurements were fractured in liquid nitrogen. The surface coating was not applied.

The composite's fractured surfaces were examined using an SEM Hitachi Tabletop Microscope TM3000 (Japan); the results can be seen in Sections 3.2 and 3.4. The composite specimens were fractured using liquid nitrogen and used as they were, to obtain images in different magnifications with a voltage of 10–15 kV. The surface coating was not applied.

For MCC powder sample (Section 2.1), TS Vega Tesca5136M (Czech Republic) was used with a voltage of 15 kV. The surface coating was not applied.

Tescan Mira\LMU (Czech Republic) was used to visualize the nanocomposites' surface morphology prepared with a fracture in the liquid nitrogen for the results section (Section 3.3). An acceleration voltage of 5 kV was used for image generation, while the specimens were fixed on standard aluminum pin stubs with an electrically conductive double-sided carbon tape. The surface coating was not applied.

Tensile testing

Tensile tests were performed at room temperature on a universal testing machine Tinius Olsen model 25ST (USA), equipped with a load cell of 5 kN at 0.2 $mm \cdot min^{-1}$ crosshead speed. Dumbbells samples were dried in a vacuum oven for 12 h at 60 °C and successfully pre-conditioned overnight under the environmental conditions of measurement. Ten parallel measurements were performed for each composite at room temperature and ambient conditions.

For water immersion tests, the samples were inserted in the distilled water and kept at 25 °C in the thermostat for 25 or 50 days, followed by removal from water and pre-conditioned overnight under the environmental conditions before measurement. Five parallel measurements were performed for each sample.

Disintegration under composting conditions

The composite material's disintegration degree was studied under aerobic simulated composting conditions at 58 °C and water content at 50 wt.%. Thin films were cut into the sample shapes (25 mm × 25 mm x 0.10 mm), and 5 samples for each composition were sandwiched between sieves. Specimens were submerged at a depth of 5 cm in a commercial compost soil consisting of local Latvian swamp peat (Formoss, Latvia) and packed in plastic containers. The range of pH values from 5.7 to 6.3 was obtained from the measurements. The laboratory-scale test was used to determine disintegration, and before the measurements, specimens were vacuum dried.

3. RESULTS AND DISCUSSION

The development and research of polybutylene succinate/cellulose composite materials were divided into four parts, which are reflected in the chapters of the Thesis. The first part focuses on the use of recycled cellulose as a cheap filler derived from waste. Recycled cellulose was used after shredding without any further treatment and mixed in a range of 10 to 50 wt.% with PBS. The data presented in this chapter allowed to understand the optimal choice of the amount of filler for further research.

In the second part smaller cellulose particles, such as microcrystalline cellulose and nanofibrillated cellulose, are used. The particle size of MCC is about 10 times smaller than previously used recycled cellulose and is close to the size of wood flour (a popular waste product). But NFC is one of the most relevant and popular nanofibers of natural origin, which is already being produced in relatively large quantities in various pilot plants. NFC was freeze-dried from an aqueous solution, thus simplifying the composite manufacturing process. The results obtained with freeze-dried NFC did not yield the expected benefit, so in-depth studies were performed in the next part.

When considering the possibility of forming PBS/NFC composites, two methods were chosen: the solution method, widely used in the literature for sample preparation, and the masterbatch process, which is suitable as an industrial production method. Furthermore, the loading of NFC was reduced to a maximum of 15 wt.% to avoid agglomeration. The author investigated the amount of NFC that could be added to the polymer to improve the properties of the composite and how this process could be combined with the production of industrially viable thermoplastic polymer composites. The use of NFC, unlike the fillers discussed above, could increase rather than reduce the cost of composite material, but it is possible to obtain unique applications and excellent properties that are not provided by micro-sized fillers.

The fourth part deals with a more complex variant of composite production, which involves adding a modifier to the polymer and cellulose system. A high loading of filler (70 wt.% MCC) was chosen to maximize the impact on the properties depending on the type of modification. Modification can make the production process more expensive and complex, so it can be justified by reducing the required mass fraction of bioplastic. As an additional benefit from the modifications, the possibility of regulating the rate of biodegradation of composite materials was observed.

3.1. Sustainable tetra pak recycled cellulose/poly(butylene succinate) based woody-like composites for a circular economy

Material processing and composite formulations

The PBS/rCell composites were processed by melt compounding with Brabender® Mixer 50EHT thermoplastic mixer. The screw rotation speed was set to 60 rpm, heating – at 130 °C for all zones, and mixing time – 5 min. Altogether, five compositions were obtained: PBS/rCell composites 10, 20, 30, 40, 50 wt.% of rCell. The materials are characterized by the recycled

component 0–50 wt.%, bio-based component 50–100 wt.%, and bio-based carbon content 50–75 % (see Table 3.1). The processed composite materials were cut into pieces and compression molded with Carver CH 4386 to obtain film specimens. The processing was done at 140 °C; granules were preheated for 2 min and compressed under 3 metric ton pressure for 3 min followed by rapid cooling between thick steel plates with the total weight of 30 kg. The injection molding was performed with previously granulated composite, and the temperature was set at 190 °C for all heating zones.

Table 3.1

The Prepared PBS/rCell Composites and their Bio-based Carbon Content

Sample	Recycled component, wt.%	Bio-based component, wt.%	Bio-based carbon content, %
PBS	-	100	50
10rCell	10	90	55
20rCell	20	80	60
30rCell	30	70	65
40rCell	40	60	70
50rCell	50	50	75

Determination of the structural properties

Table 3.2

Vickers Micro Hardness, Theoretical Density, and the Experimental Density of Pristine PBS and PBS/rCell Composites.

W_{rCell}, wt.%	φ_{rCell}, vol.%	d_p, g/cm^3	d_t, g/cm^3	Δ, %	d_{poly}, g/cm^3	H_V, MPa
0	0	1.365	1.365	0	1.365	255±31
10	15	1.337	1.386	3.6	1.308	567±40
20	30	1.329	1.406	5.6	1.256	490±60
30	45	1.323	1.426	7.5	1.179	488±19
40	60	1.320	1.446	9.2	1.050	431±15
50	75	1.313	1.466	11.2	0.752	365±50

Figure 3.1 shows (a) typical example of (a) obtained optical microscopy (b) SEM images of rCell, (c)–(d) rCell size distribution, (e) PBS/rCell composite optical microscopy, and (f) SEM images. As it was previously stated, rCells are characterized by average length − 200 μm and average width − 20 μm. The microstructure of the PBS/rCell composite is shown in Fig.1(f). Table 3.2 summarizes the percentage of weight content of cellulose (W_{rCell}), percentage of volume content cellulose (φ_{rCell}), Vickers microhardness (H_V), theoretical density (d_t), the apparent polymer density (d_{poly}), and the experimental density (d_p) calculated according to descriptions in the methods section.

It corresponds well with the observed decrease of measured experimental composite density and calculated polymer apparent density (see Table 3.2). The rule of mixtures was used to calculate the theoretical density of the composites and used as a reference [38]. The polymer structure can be described by the apparent density d_{poly} of the polymer. The polymer density contribution in the composite is calculated similarly as in [39] and according to the equation

$$d_{poly} = \frac{d - d_{Cel} \cdot \varphi_{Cel}}{1 - \varphi_{Cel}}. \qquad (6)$$

The PBS/rCell's experimental density decrease could be caused by the possible agglomeration of cellulose particles and the formation of voids and defects in the composite microstructure by rCell particles addition, as can be seen in Fig. 3 (f) and reported in the literature [40], [41].

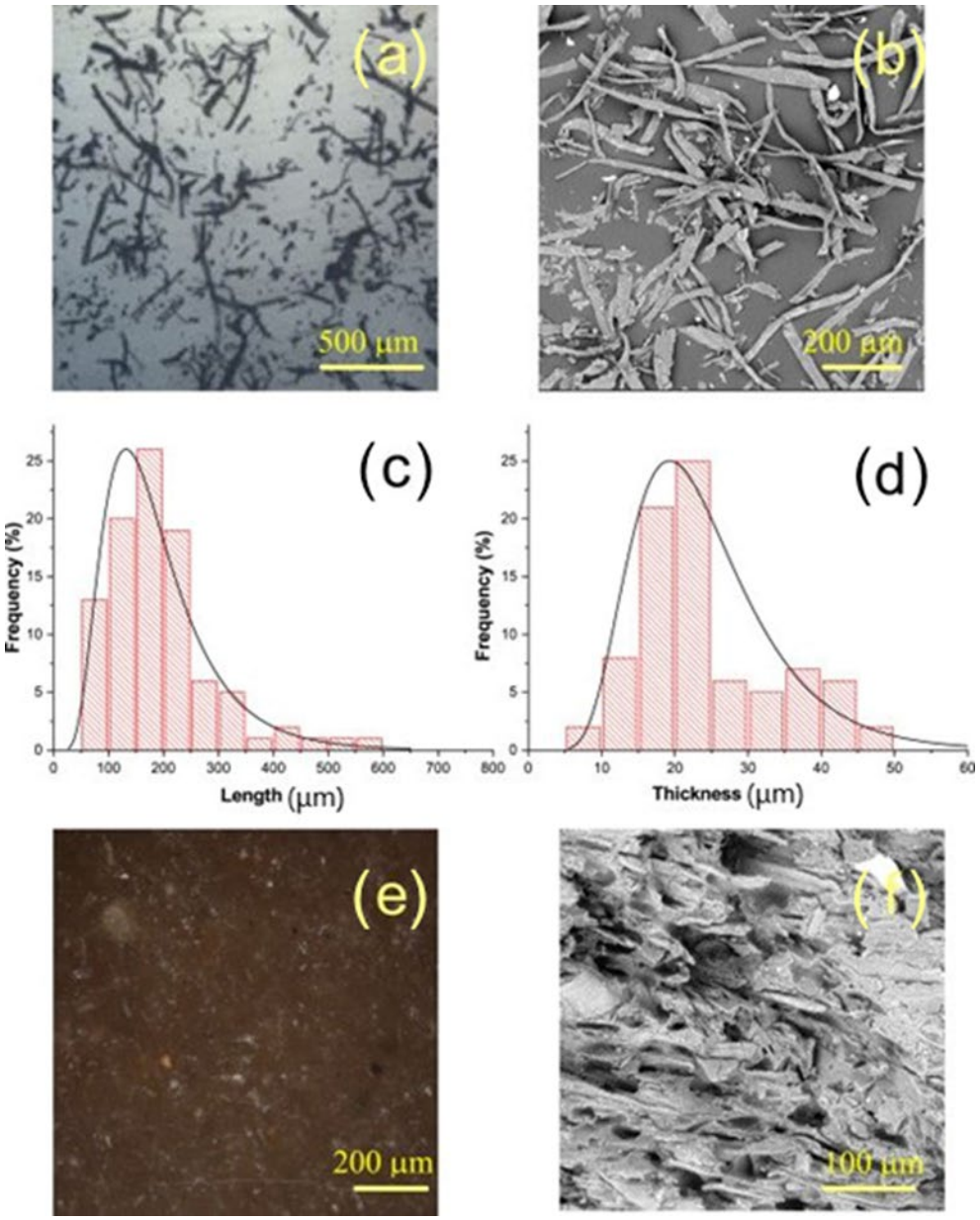

Fig. 3.1. rCell particles: (a) optical microscopy image, (b) SEM image; rCell size distributions: (c) length, (d) thickness; 40rCell composite: (e) optical microscopy image, (f) SEM image.

Determination of filler and matrix interaction

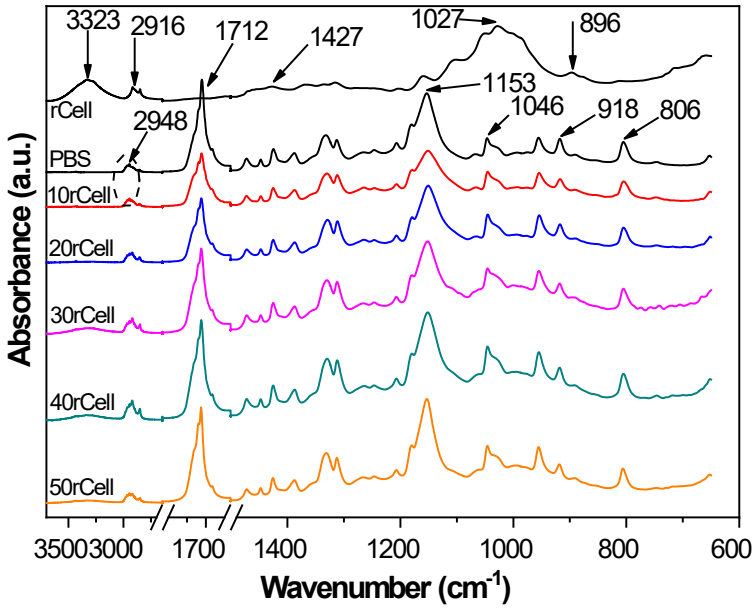

Fig. 3.2. FTIR spectra of PBS/rCell composites.

The FTIR spectra of the prepared PBS/rCell composites is shown in Fig. 3.2. The characteristic spectra for aluminum and polyethylene residues in the ground tetra pak rCell filler were not observed in the obtained FTIR spectra that testify good purity of the rCell filler. FTIR spectra PBS/rCell composites of the different compositions had a similar shape. The stretching vibration of the cellulose OH group was at the peak at 3323 cm^{-1} [42]. FTIR absorption band at 896 cm^{-1}, assigned to C–O–C stretching at β-(1α4)-glycoside linkages, is designed as an "amorphous" absorption band, an increase in its intensity occurring in the amorphous cellulose [43]. The presence of methylene groups in the PBS backbone is described as stretching vibration at 2948 cm^{-1} [44]. While 1712 cm^{-1} region is attributed to C=O stretching vibrations of the ester group in the crystalline domain and the peak located at about 1738 cm^{-1} is C=O stretching in the amorphous region [45]. The peak at 1153 cm^{-1} is assigned to the asymmetrical stretching vibration of the C-O-C bond, and the bands at the 1046 cm^{-1} region were assigned to O–C–C stretching vibrations [44], [46]. While the bands at 918 and 806 cm^{-1} have been attributed to bending vibrations of C-OH from the carboxylic acid group [44]. The peak close to 2900 cm^{-1} was observed for the cellulose with the experimental measurement at 2916 cm^{-1} and was attributed to C-H stretching vibrations, and it can clearly be differentiated from PBS backbone absorption described above [47]. FTIR absorption peak intensity at 1427 cm^{-1} was assigned to asymmetric CH_2 bending vibration of the crystalline chain domains.

Mechanical properties and effect of immersion in water

The loading of 10 wt.%. of rCell into the PBS has resulted in almost a 2-fold improvement of the hardness values (see Table 3.2). The hardness value decreases gradually with rCell loading up to 50 wt.% into the polymer. This observation well corresponds to the common forms of the defects, the voids and the heterogeneities in the polymer/cellulose composite material with high cellulose filler loadings [48]. The elasticity of the composites showed a tendency to increase significantly as higher amounts of cellulose are mixed into the PBS/rCell

composite. This is in line with previous wood polymer composites studies [49]–[51]. The prepared PBS/rCell composites have a remarkable enhancement in Young's modulus E (Fig. 3.3 (a)). The E value rises almost monotonically with the higher rCell content. It indicates an almost 2-fold increase and a 3-fold in E for the samples containing 30 wt % and 50 wt.% of the rCell. The tensile strength at break σ decreases significantly after the rCell filler incorporation (Fig. 3.3 (b)). The composition with the 50 wt.% of rCell showed a 2-fold decrease of the σ value. The ductility of the composite, expressed as tensile strain at break ε, decreased from 30 % to 3 % when rCell loading reached 50 wt.%. This observation is common for polymer composites filled with cellulose loading above 20 wt.% [52]. The received data indicates that the quality of cellulose-based structures is significantly impacted by moisture content [53]. It results in some decrease in the ductility and some depress in the elasticity, while the strength of the composite remained almost unchanged after 50 days of immersion in water tests. Drop in the composite ductility can be facilitated by swelling and subsequent shrinking of the cellulose particles during the immersion and drying steps [54].

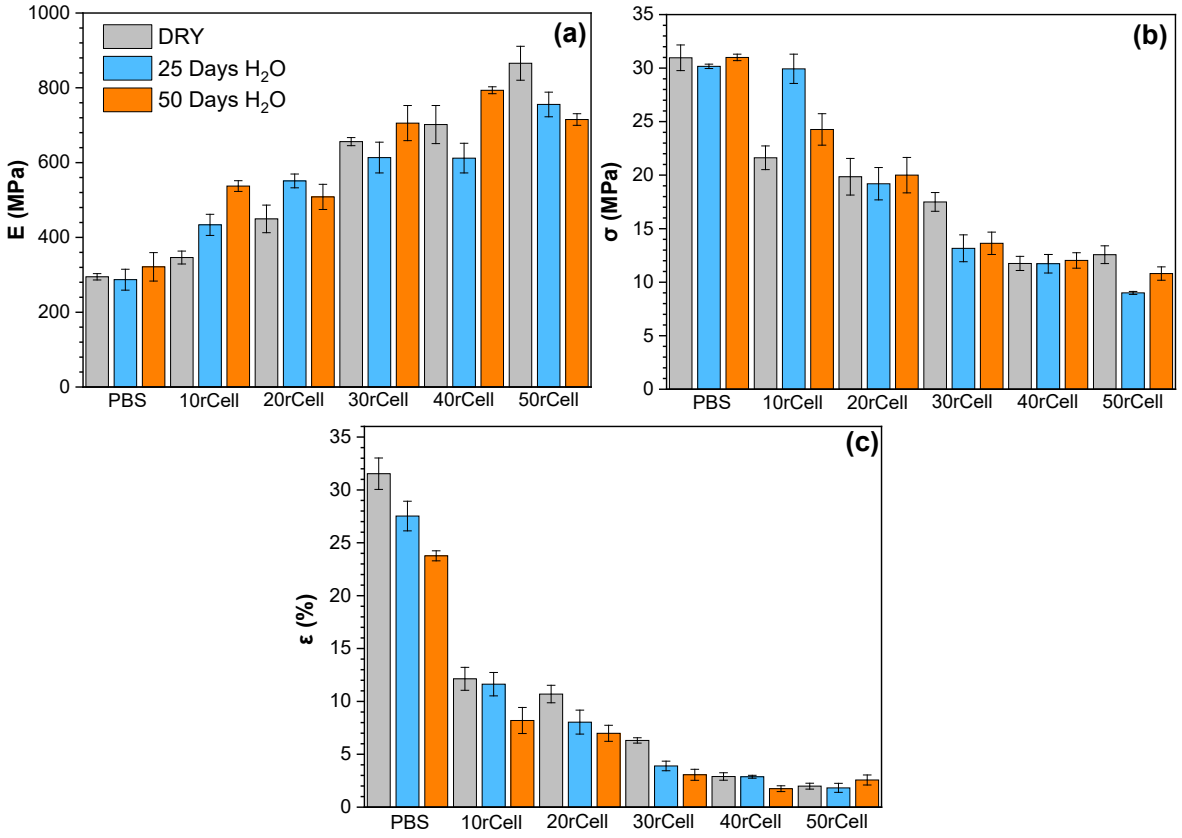

Fig. 3.3. Tensile properties for PBS/rCell composites: (a) Young's modulus *E*; (b) tensile strength σ; (c) strain ε.

Crystallization behaviour of composite

Figure 3.4 presents the DSC of (a) second heating and (b) cooling of the PBS and the PBS/rCell composites. The results for the melting temperature (T_m), crystallization temperature (T_c), the crystallinity from the second heating melting peak (χ_m) and the crystallinity from the crystallization peak (χ_c) are reported in Table 3.3. A broad melting peak is identified from

almost 90 °C and reaches 125 °C for the neat PBS. Melting temperature T_m of the PBS is 114 °C.

Table 3.3

Thermal Properties of PBS/rCell Composites

Sample	T_m, °C	T_c, °C	χ_m, %	χ_c, %	$T_{10\%}$, °C	$T_{50\%}$, °C	T_{deg}, °C
rCell	-	-	-	-	317	484	340
PBS	114	81	65	63	366	395	397
10rCell	115	88	43	45	363	397	401
20rCell	116	89	32	36	354	395	401
30rCell	118	90	27	26	353	397	405
40rCell	117	90	18	19	344	394	402
50rCell	115	90	16	14	329	384	392

The cellulose loading does not affect the T_m of the composite material. The presence of the cellulose particles commonly induces the nucleation of the polymer chains and the formation of the trans-crystalline phase on the cellulose surface [55]. The crystallization peak of the composites increases almost by 9 °C; T_m shifts to the higher temperatures from 81 °C for the PBS to up to 90 °C for the PBS/rCell 30 wt.%. The polymer composite crystallization also starts at higher temperatures than for the neat polymer. However, the crystallinity χ_m and χ_c values revealed an apparent decrease when rCell was incorporated into the PBS matrix. The addition of more than 10 wt.% of cellulose components could destroy the crystallinity of PBS polymer [56]. The strongly disrupted polymer chain mobility in the cellulose's interface significantly disrupts the crystals' growth in the PBS/rCell composite.

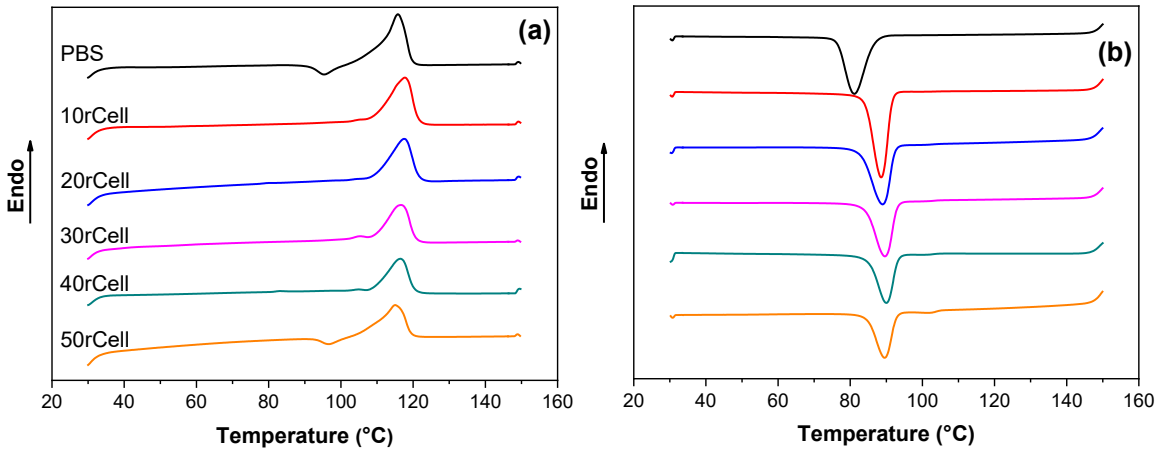

Fig. 3.4. DSC curves of PBS/rCell samples: (a) second heating, (b) cooling.

Investigation of thermal stability

TGA was used to investigate the thermal sensitivity and degradation properties of PBS/rCell composite materials and the influence on composition with the increased filler content. Figure 3.5 showed TGA (a) and DTG (b) curves of PBS/rCell composites. Table 3.3 summarizes the

TGA data from which $T_{10\%}$ represents the temperature of thermal degradation for 10 % weight loss, $T_{50\%}$ represents the temperature of thermal degradation for 50 % weight loss, and T_{deg} represents the temperature at maximum weight loss rate. It reveals that the maximum degradation temperature for rCell is 340 °C and the neat PBS is 398 °C. The cellulose incorporation induces lowered thermal stability for the composites [57], [58]. The PBS curve shows a single-stage degradation. The degradation of PBS starts with a small weight loss above 200 °C, which has been attributed to the degradation of oligomers present in PBS, while the main degradation of PBS starts at around 350 °C and is explained by a random cleavage of the ester bond due to the transfer of hydrogen atom from β-CH [59]. In turn, the PBS/rCell composites show similar thermal behaviour, except for PBS/rCell 50 wt.% having a two-stage degradation, which is indicated in the DTG curve. The thermal degradation process of the composites is defined primarily by the PBS polymer chain degradation, while the PBS/rCell 50 wt.% composite is affected by the cellulose thermal degradation. With the increase of the cellulose content, it can be observed that the curves shift to lower temperatures. This is pronounced when $T_{10\%}$ is observed for 50rCell, which is 329 °C, resulting in a 37 °C decrease compared to pristine PBS. If we take $T_{50\%}$ into consideration, 50rCell stands out having 10 °C lower temperature compared to PBS and other composites. The thermal degradation temperature T_{deg} is 397 °C, while T_{deg} remains almost unaffected by the rCell content in the composite materials.

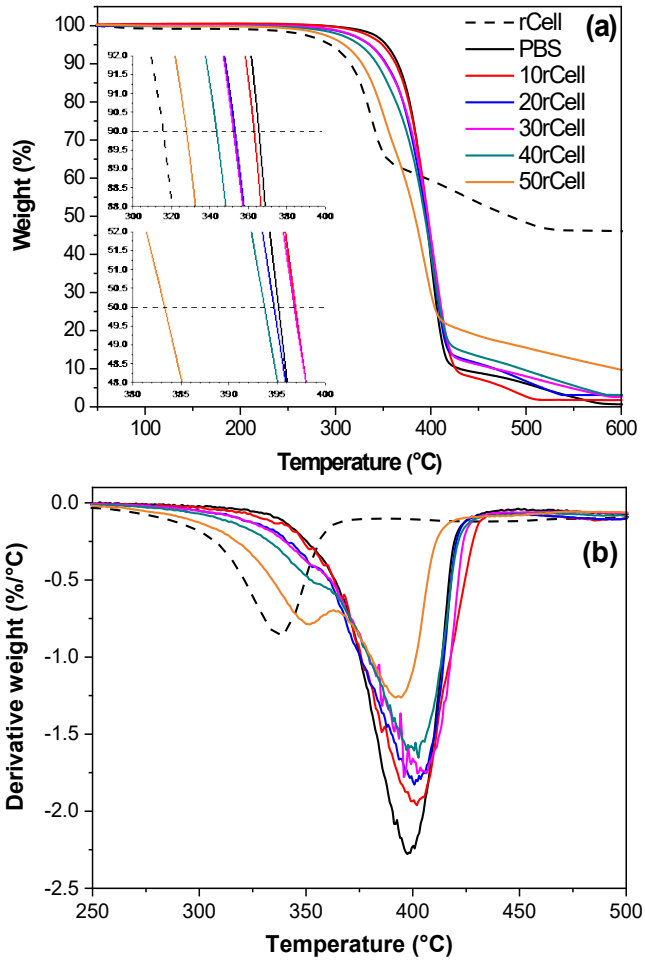

Fig. 3.5. (a) TGA curves and (b) DTG of PBS/rCell composites.

Investigation of viscoelastic properties

Viscoelastic properties of the PBS/rCell composites were investigated by dynamic mechanical analysis. Storage modulus *E*', loss modulus *E*'' and the loss factor tan δ as a function of temperature are shown in Fig. 3.6. The results show a tremendous increase in the measured viscoelastic characteristics (*E*', *E*'', tanδ) in all investigated temperature range. As more rCell content is loaded into the polymer, the respective improvement of composite properties to store energy reversibly, transformed energy irreversibly, and to dissipate energy is to a greater extent related to the reinforcing effect of the used filler. The increase of the content of the fiber filler featured that a high geometrical dimensions aspect ratio improves reinforcing efficiency significantly [60]. For example, in the case of rCell loading 50 wt.%, composites *E*', *E*'', and tanδ at room temperature (20 °C) have increased about 3, 6, and 2-fold, accordingly. While loss modulus *E*'', which characterizes the dissipated energy into heat and loss, has a maximum at the temperature range of –40 to 10 °C. The relative heights of the loss factor tanδ are proportional to the energy dissipation property of the material. It shows at temperature –10 °C almost a 30 % decrease in tanδ value for the composites with rCell content 20–50 wt.%. Compositions 20rCell, 30rCell, 40rCell, and 50rCell show enhanced values of *E*', *E*'' in the whole measured temperature range, meaning that well-dispersed fiber network and reinforcement is established.

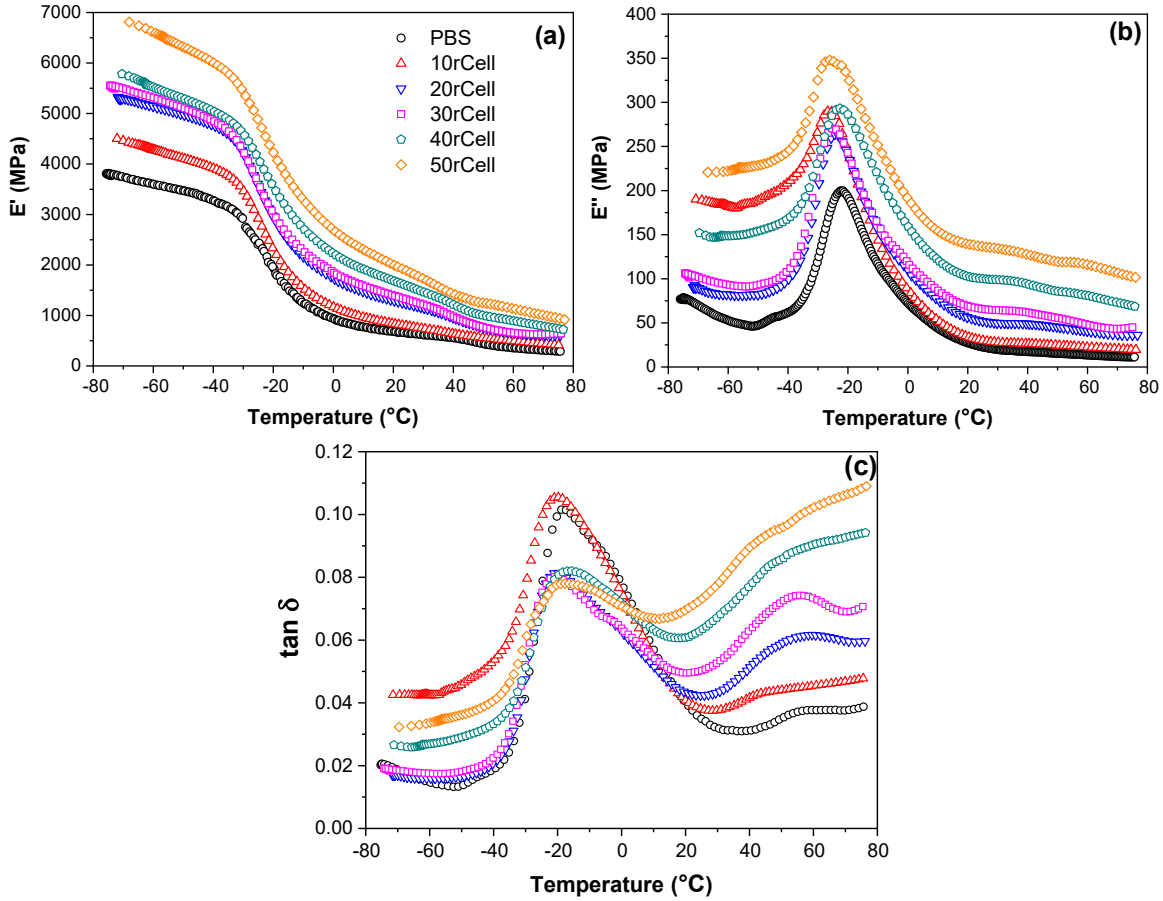

Fig. 3.6. DMA curves of PBS/rCell samples: (a) storage modulus *E*', (b) loss modulus *E*'', and (c) loss factor tan δ.

Determination of the compositing performance

Degradation of the PBS and PBS/rCell composites under the composting conditions were used to evaluate the disintegrability in natural environments. The visual evaluation of the samples at different degradation times is shown in Fig. 3.7. Considerable changes in visual appearance of all samples were obtained already after 10 days. At the same time, the composite samples compared to the neat PBS showed evident brittleness and size reduction after 30 days. After 70 days of evaluation, all the samples were completely degraded under the composting condition at 50 °C. A clear decrease in the degradation time is observed for the PBS/rCell composites in comparison to the neat PBS. The higher content of biodegradable cellulose in the material strongly facilitates the degradation of the PBS/rCell composites. This contribution relates to the quicker water absorption from the composting medium, resulting in an evident increase in disintegrability values for the composite samples. Similar observations were reported in [11], [61]. The observed decrease in the crystallinity of the polymer matrix also could forward the degradation and disintegrability of the composite samples. Fortunati et al. indicated that the polyester hydrolysis begins in the intrinsic amorphous regions of the polymer and significantly accelerates the degradation of the polymer material [62]. Similar behavior of progressive degradation of samples after loading with the cellulose fillers was also reported by several researchers in [62]–[64]. Finally, it was observed that after 70 days of the degradation test, all samples reached complete degradation. These observations testified the possible application of the processed composite materials as biodegradable materials with disintegration times up to 70 days in controlled environmental conditions.

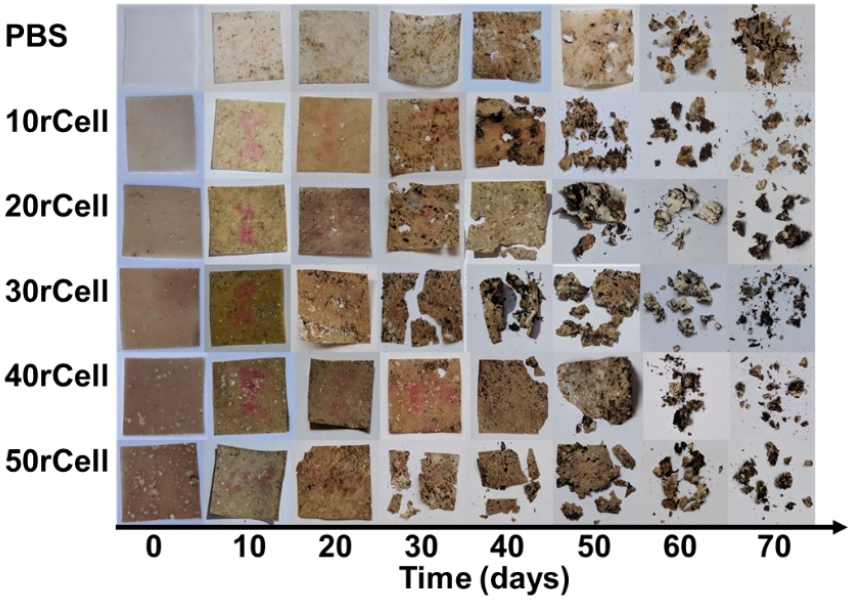

Fig. 3.7. Photos of PBS/rCell composite films during biodegradation studies in soil burial test conducted in composting conditions.

Summary

This study investigates the performance of woody-like composites consisting of the bio-based poly(butylene succinate) and 10–50 wt.% recycled cellulose obtained from the industrial

Tetra Pak processing plant. Based on the experimental results, the following conclusions are presented:

1. The addition of 50 wt.% of rCell into PBS leads to a 2-fold improvement in the hardness of the composite compared to the neat PBS. The Young's modulus increases almost 3-fold, the storage modulus – 4-fold, and the loss modulus – 6-fold in room temperature, while tensile strength and ductility decrease correspondingly.
2. The PBS matrix effectively shields the filler, enhancing the thermal stability of the rCell composites. Single step thermal degradation was observed for rCell loadings up to 40 wt.%. The crystallinity of the polymer, calculated from DSC curves, decreases with rCell wt.% content, but the increase in the crystallization temperature indicates that cellulose induces the nucleation of the polymer chains.
3. All composites degrade in composting conditions within 70 days.
4. Mechanical properties for samples immersed in water remained almost unchanged after 50 days, thus indicating suitability for WPC applications.

3.2. Bio-based poly(butylene succinate)/microcrystalline cellulose/nanofibrillated cellulose-based sustainable polymer composites: Thermo-mechanical and biodegradation studies

Material processing and composite formulations

PBS was dried in a vacuum for 5 hours in 80 °C according to manufacturer's recommendations. MCC and NFC in the form of powders were dried in a vacuum for 24 hours in 60 °C. The composites were prepared with Brabender® Mixer 50EHT with the blending temperature set at 140 °C and the rotation speed at 70 rpm. The pure PBS sample was processed; 5 composites were prepared with 40 wt.% of MCC, NFC and MCC/NFC combinations in the PBS matrix. The prepared compositions are summarized in Table 3.4.

Table 3.4

The Prepared PBS/Cellulose Compositions

Sample	PBS, wt.%	NFC, wt.%	MCC, wt.%
PBS	100	0	0
40NFC	60	40	0
40N7/M3	60	28	12
40N5/M5	60	20	20
40N3/M7	60	12	28
40MCC	60	0	40

Carver CH 4386 hydraulic press was used to prepare thin films having a thickness of 0.1 mm and 0.3 mm for tests. Mini-Jector #55-1E injection moulding device was used to prepare dumbbells shaped samples for tensile tests. Compression moulding was performed at a temperature of 140 °C for 5 min and 3 metric ton of pressure, followed by rapid cooling to room temperature between thick steel plates. Injection moulding device was set at the temperature of 190 °C, and samples were cast in the steel moulds.

Thermal properties

Figure 3.8 shows the weight loss and the derivative weight loss curves of the pristine PBS, composites, and NFC, MCC fillers. NFC starts to degrade faster and has a narrower degradation peak, and it loses less of its overall weight compared to MCC; this could be attributed to the NFC structure that includes fibrils of varied nano sizes. PBS effectively shields the cellulose filler, increasing composite thermal degradation at 50 % weight loss by 60 °C compared to MCC and NFC. Compared to pristine PBS, the thermal stability of composites was reduced. Weight loss curves indicate that cellulose has lower thermal stability and both NFC and MCC are similar and shows maximum weight loss at around 320 °C, while PBS has much higher temperature at 406 °C. The initial weight loss for the cellulose samples at around 100 °C has been attributed to the bonded water, while the cellulose carbon skeleton pyrolysis starts at around 300 °C [65]. Table 3.5 summarizes the TGA data from which $T_{5\%}$ represents the thermal degradation temperature for 5 % weight loss, $T_{50\%}$ represents the temperature of thermal degradation for 50 % weight loss, T_{max} represents the extreme weight loss rate temperature.

The thermal stability of 40NFC composite was by 18 °C lower at $T_{5\%}$ compared to 40MCC, and composition 40N3/M7 had the highest degradation temperature at 305 °C, proving 25 °C and 7 °C increase respectively compared to single type cellulose specimens. For the values of $T_{50\%}$ and T_{max}, all compositions showed similar values, except for the 40MCC sample which had a 10 °C lower maximum weight loss temperature compared to other composites.

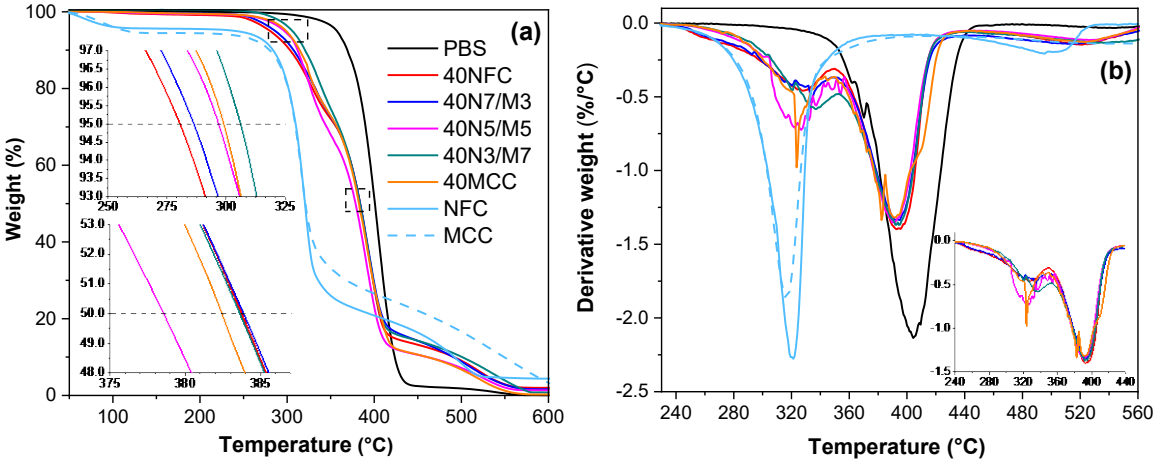

Fig. 3.8. (a) Thermogravimetric analyses contours and (b) differential thermogravimetric contours of PBS, PBS/cellulose composites, NFC and MCC under air atmosphere.

Table 3.5

Thermal Properties of PBS/Cellulose Composites

Sample	$T_{5\%}$, °C	$T_{50\%}$, °C	T_{max}, °C	T_m, °C	T_c, °C	H_m, J/g	H_c, J/g	χ_c, %
PBS	356	400	406	114.2	75.3	75.1	72.9	66.0
40NFC	280	384	392	114.2	81.9	31.8	35.0	52.8
40N7/M3	286	384	392	115.1	88.1	34.5	36.8	55.4
40N5/M5	296	379	392	115.8	89.0	37.7	37.2	56.1
40N3/M7	305	383	395	115.8	87.6	39.0	38.2	57.6
40MCC	298	382	383	116.5	85.2	38.8	42.6	64.2

DSC experiments were used to analyse the thermal and crystallization properties of PBS/cellulose composites. Table 3.5 displays the summary of different thermal properties (e.g., crystallization temperature (T_c), melting temperature (T_m), crystallization enthalpy (H_c), melting enthalpy (H_m)), while the crystallization and melting curves are shown in Fig. 3.9. Pristine PBS exhibited a sharp crystallization peak and crystallization temperatures (T_c) at 75.3 °C. The addition of NFC shifted crystallization temperature to 81.9 °C, while the addition of MCC continued to enhance the crystallization temperature to 85.2 °C, but for the NFC/MCC filler compositions, even higher values were observed of which the 40N5/M5 composition crystallization peak was at 89.0 °C. While the crystallinity degree χ_c decreases with the addition of cellulose fillers from 64.2 % for 40.0MCC down to 52.8 % for 40.0NFC, NFC/MCC follow the same trend with higher NFC content resulting in lower overall material's crystallinity. It has been reported that the structure of cellulose fillers impacts the crystallization process, while the agglomeration of NFC filler lowers crystallinity [66]. Thus, the degree of crystallization χ_c increases by higher MCC content indicating heterogeneous nucleation of PBS matrix [67], while

observed the different values of crystallinity for 40NFC and 40MCC composites indicate strong dependence on the structure of cellulose filler. The observed curves indicate the polymer crystal nucleation by both fillers and pronounced trans-crystallization that can be observed as splitting in the melting peak [68].

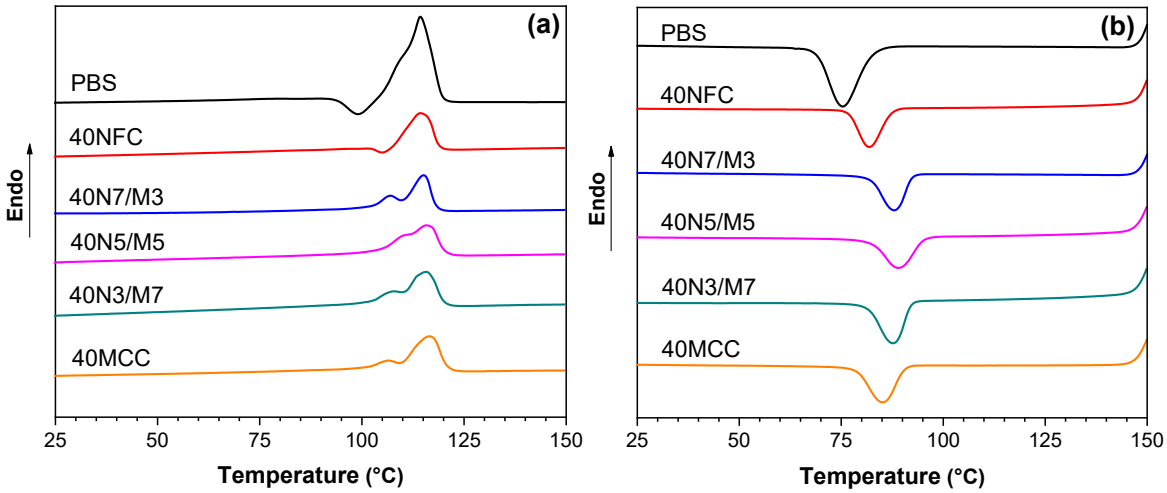

Fig. 3.9. (a) Melting peaks of the second heating and (b) crystallization peaks of PBS and PBS/cellulose composites under the nitrogen atmosphere.

Thermomechanical and tensile properties

The thermo-mechanical properties of the PBS composites were studied with DMA. As evident from Fig. 3.10 (a), the storage modulus of the prepared composites increases significantly with the addition of cellulose fillers to the PBS matrix. The storage modulus was increased from 66 % up to 119 % at 20 °C with the lowest result for 40N7/M3 composition and highest for 40MCC, which showed the best enhancement in the whole temperature range compared to PBS. Similar trends were obtained for the loss modulus peaks (Fig. 3.10 (b)), which indicated the increase in the composite dampening properties, with an increase from 75 % up to 100 % at 20 °C, with 40MCC having the highest observed value and 40N7/M3 the lowest compared to PBS. But before the glass transition temperature, composition 40N5/M5 showed a significantly higher loss modulus than the rest of the composites. The storage and the loss modulus had an increase in the entire temperature array, indicating a good filler dispersion and existing reinforcement network through the whole composite and good load-bearing properties [69]. The loss modulus increase can be explained by the particle-particle slippage, in this case cellulose filler and polymer PBS matrix that dissipated more heat than pure PBS [70]. The glass transition values as seen in tan δ peak (Fig. 3.10 (c)) ranges from -21 °C to -16 °C and are relatively unchanged for the composites compared to PBS value that was -16 °C. The absolute values of tan δ peak that characterize the energy dissipation were slightly decreased, resulting in lower energy requirement for viscoelastic deformation of the composites, indicating weak interactions between the PBS matrix and NFC/MCC fillers [71]. Thus, the storage and the loss modulus increase could be explained by the rigid MCC and NFC fibres proving the enhancement and reinforcement network.

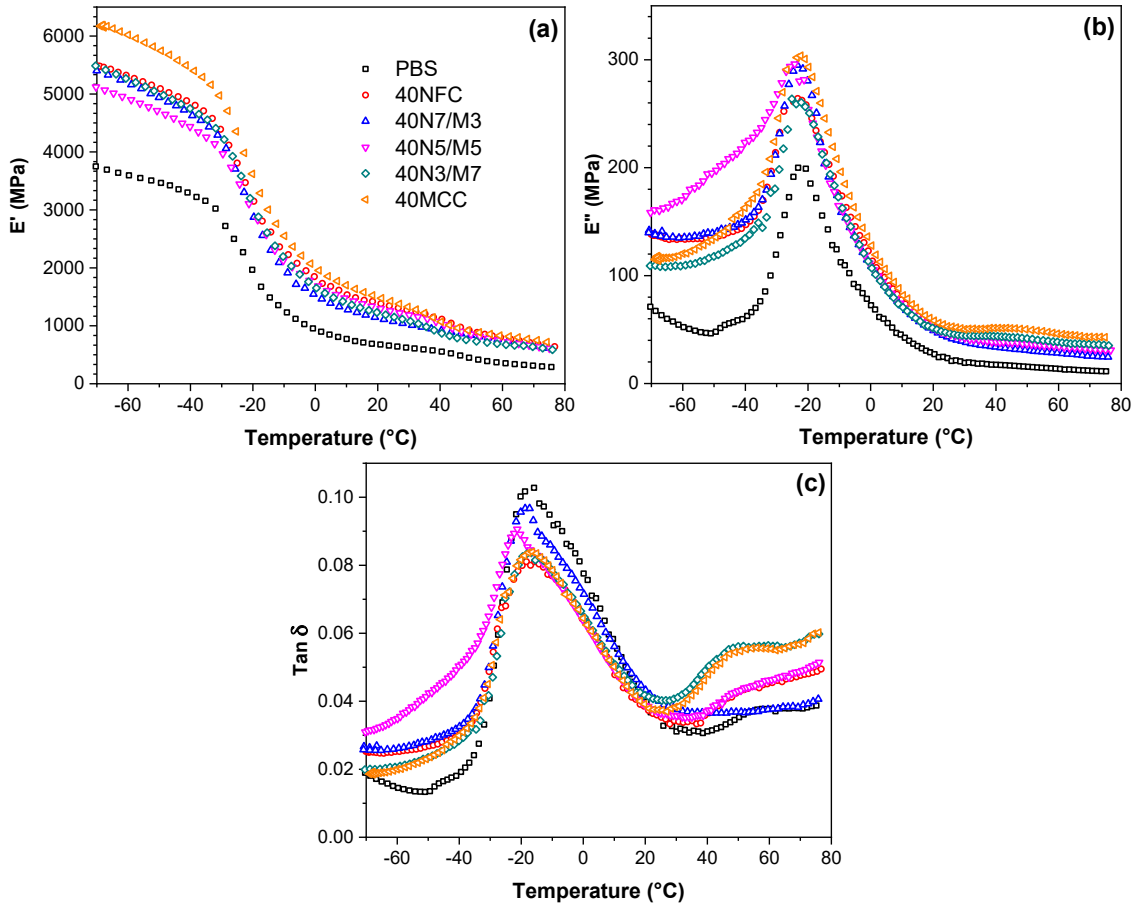

Fig. 3.10. (a) Storage modulus *E*'; (b) loss modulus *E*''; and (c) loss tangent tan δ curves of PBS and PBS/cellulose composites.

Figure 3.11 shows the mechanical properties for PBS/cellulose composites tested in tension mode. The addition of the cellulose fillers to the PBS matrix causes an increase from 271 MPa to 561 MPa (107 % increase) for 40NFC with the highest value 626 MPa (131 % increase) for 40N5/M5 in Young's modulus, and this could be attributed to the inherited high modulus value of cellulose. The difference between filler crystallinity with similar composition has been shown to impact Young's modulus and could explain higher values achieved with compositions that have higher MCC content [72]. Synergic effect of the fillers has been observed for 40N5/M5 composition, while 40NFC and 40N7/M3 compositions showed the lowest Young's modulus. A decrease has been observed for tensile strength from 30.9 MPa for PBS down to 22.5 MPa for 40MCC and the lowest value 12.9 MPa for 40NFC, which is a similar situation for the elongation values, as 40MCC has the highest observed at 5.11 % and 40NFC the lowest – 3.18 %. A decrease in tensile strength can directly be attributed to weak interactions between the filler and matrix [72]. This results in stress concentrations that lead to brittle points in the composite's structure that reduce tensile strength and elongation values [73], [74]. While from hybrid compositions, the highest tensile strength was observed for 40N3/M7. Thus, it can be observed that NFC shows poorer mixing with PBS matrix compared to MCC, and this could be attributed to different structures, surface area and crystallinity of cellulose, which affects the amount of available OH groups and increase chemically bound water [75]. Ductility decrease

has been explained by the increased volume of cellulose with high loading that enlarges the contact surface, which results in restricted polymer chain movements [76]. That is commonly observed as a sharp decline in elongation and has been reported for PBS/plant fibre compositions [77], [78] and other polymers like polypropylene/wood composite systems [76], [79].

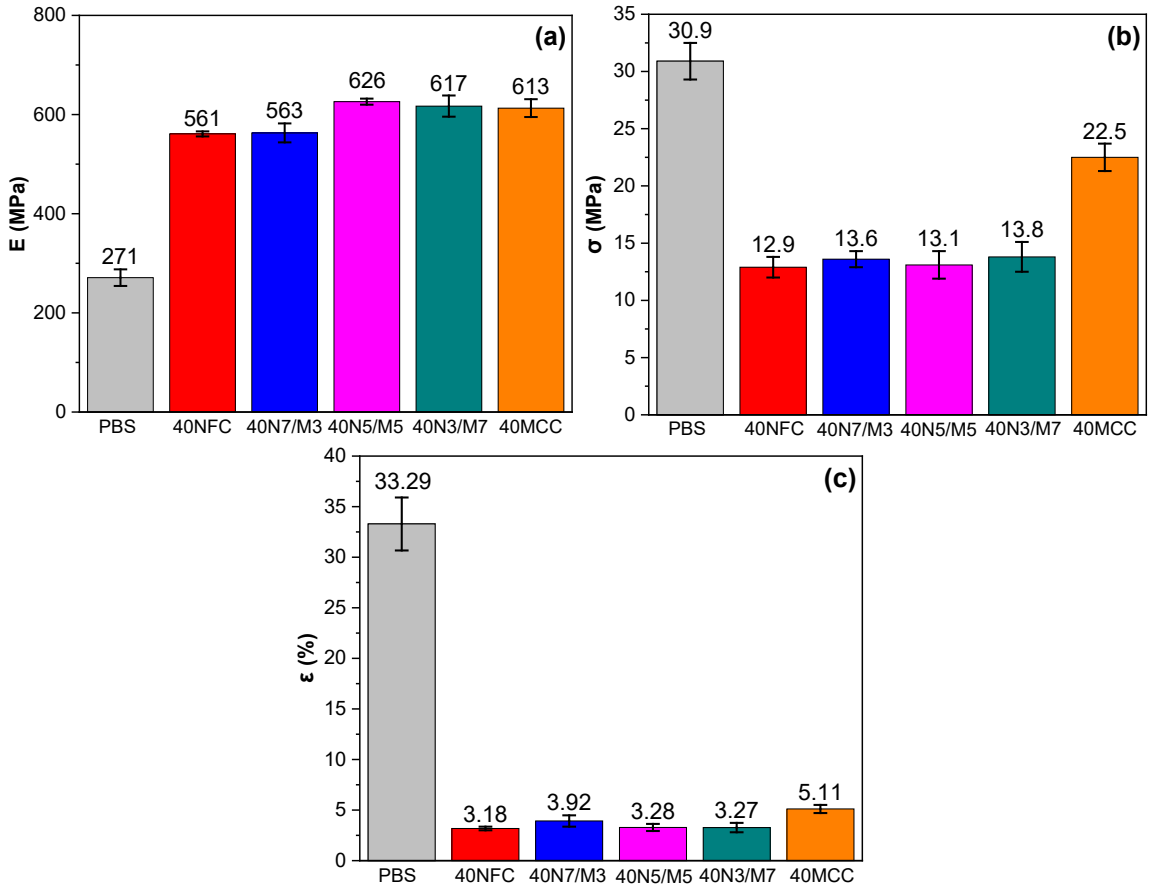

Fig. 3.11. Tensile strength results of PBS and PBS/cellulose composites: (a) elastic modulus *E*; (b) tensile strength σ; and (c) strain ε.

Biodegradation studies in the composting conditions

Visual specimen degradation can be observed in Fig. 3.12. For the pristine PBS, it takes around 75 to 80 days to become almost indistinguishable from the soil. As seen in the case of MCC and NFC filled compositions, it takes 10 days less for them to degrade, resulting in the total time around 65 to 70 days. We also observed that PBS/cellulose composites lose their ductility much faster, become brittle, and easily crumble under slight pressure, while pristine PBS retained mechanical toughness longer. The composition with MCC showed slightly enhanced degradation compared to NFC ones. It has been reported before that a cellulose-based filler enhances the degradation of PBS in composting conditions and the weight percentage of filler determines the impact on the degradation time [13]. A hydrolysis mechanism is the first stage of PBS degradation and requires enzymatic activity in soil and water, while degradation products are processed by bacteria and fungi [80], [81]. It has been shown that the amount of water, temperature, and composition of soil influences the degradation time significantly [82], [83]. Other factors like crystallinity also impact the speed of degradation, and generally

amorphous regions of polymers degrade faster than the crystalline ones [80]. So, the result where compositions with MCC indicated faster degradation than those with more NFC could be explained by better filler distribution in the polymer matrix, as observed in SEM images. Thus, better compatibility and distribution of MCC in blend allows to further enhance the composting properties.

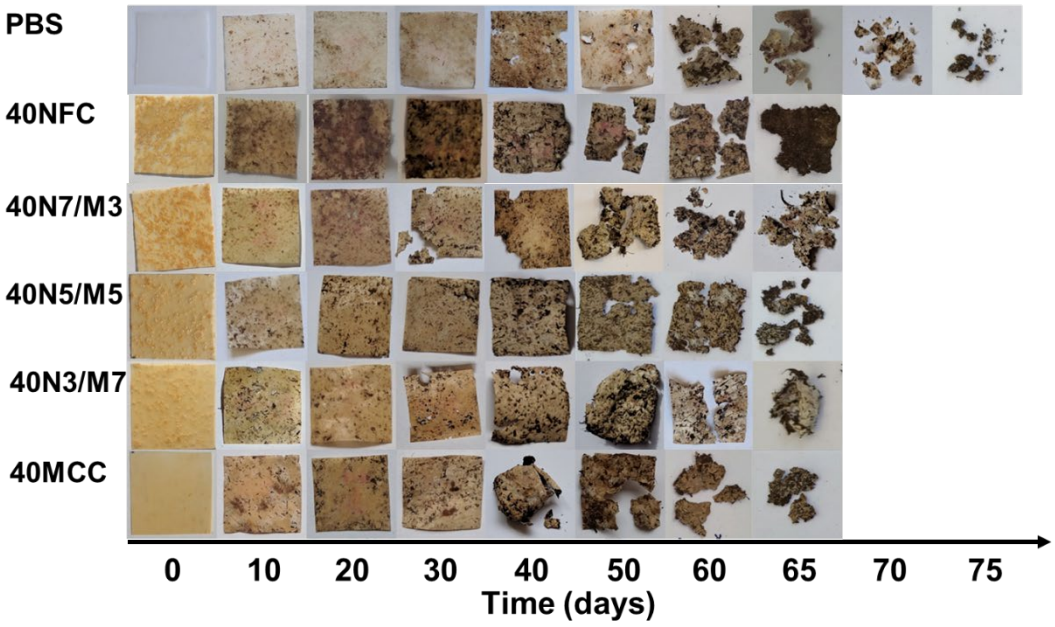

Fig. 3.12. Photos of biocomposite films during biodegradation studies in soil burial test conducted in composting conditions.

Summary

This study investigates the performance of biodegradable WPCs consisting of the bio-based poly(butylene succinate) and 40 wt.% MCC/NFC. Based on the experimental results, the following conclusions are presented:

1. The SEM images of the fracture surfaces displayed that MCC and NFC pose very different compatibilities with PBS, with MCC clearly having superior dispersion.
2. The composites' storage modulus increased significantly in the measured temperature range, confirming an effective filler reinforcement network. The tensile test showed that Young's modulus improved about 2-fold, whereas tensile strength decreased along with elongation values. The 40MCC composition had the overall best mechanical properties.
3. All composites degrade in composting conditions within 65 days.
4. For melt processing applications, MCC proved to be more suitable, while freeze-dried NFC is not recommended.

3.3. Adding value to poly(butylene succinate) and nanofibrillated cellulose-based sustainable nanocomposites by applying masterbatch process

Material processing and composite formulations

PBS granules were dried in a vacuum furnace (J. P. Selecta) at 60 °C (5 to 20 mbar) for 8 hours before further processing. NFC gel was diluted with dimethylformamide (DMF) from 11 wt.% to around 3 wt.%. To remove water, NFC was transferred to dimethylformamide (DMF) via solvent-assisted centrifugation, which was repeated 2 times, and the high shear mixer L5M-A (Silverson Machines LTD) achieved even dispersion in the solvent (2 min, 5500 rpm). PBS solution in chloroform (5 wt.%) was prepared and mixed with NFC/DMF suspension using a high shear mixer (2 min, 5500 rpm). Five samples were cast 5, 10, 15, and 50 wt.% of NFC/PBS and a pure PBS as reference. The samples were dried in ambient conditions for 2 days and inserted in a vacuum furnace for 4 hours at 70 °C to remove the remaining solvents. Sample 50 wt.% NFC/PBS was mixed with dried PBS granules in thermoplastic mixer Brabender® Mixer 50EHT (Germany) to produce 5, 10, and 15 wt.% samples. The processing conditions were adjusted to 70 rpm for twin screws, heating in all zones was 130 °C and 5 min melt compounding followed by an additional 5 min of mixing in 160 °C.

Compression molding (Carver CH 4386) was used to obtain the specimens' films with a thickness of 0.10 mm for the biodegradation test and 0.25 mm for other tests. The compression molding heating plates were set at 140 °C, while the samples were preheated for 2 min, compressed for 3 min (3 MT pressure), and cooled for 3 min between steel plates (30 kg of thermal conductive mass). To distinguish the samples, the following abbreviations were selected: 5S, 10S, 15S, used for solvent cast samples, and 5M, 10M, 15M for melt-compounded samples from masterbatch (Table 3.6).

Table 3.6

The Prepared PBS/NFC Compositions

Sample	PBS, wt.%	NFC, wt.%	Preparation
PBS	100	0	solution and melt
5M	95	5	solution
10M	90	10	solution
15M	85	15	solution
5S	95	5	masterbatch melt
10S	90	10	masterbatch melt
15S	85	15	masterbatch melt

Structural properties

Figure 3.13 shows the SEM images of selected specimen fracture surfaces in liquid nitrogen. Melt composite 5M shows a much better NFC distribution in the PBS matrix than 5S (Figs. 3.13 (a), (b)). Sample 5S shows the regions that contain almost pure polymer, while the image also shows an agglomeration of NFC. NFC shows good PBS adsorption on the fibril surface at 5 wt.% loadings. While in Fig 3.13 (c), in 15M, the NFC is dispersed evenly, fibrils

are encompassed in a polymer matrix showing no signs of being pulled out or separated from PBS. A slight agglomeration can be seen between some of the nanocellulose fibrils, but no significant defects can be observed. Unfortunately, 15S (Fig. 3.13 (d)) SEM image indicates poor filler dispersion in matrix. Also, the separation of filler and polymer matrix phases can be observed in the 15S sample. Similar SEM results were reported in the literature for PLA/NFC composites prepared by solvent casting, and the authors noted that agglomerates directly contributed to fracturing formation [84].

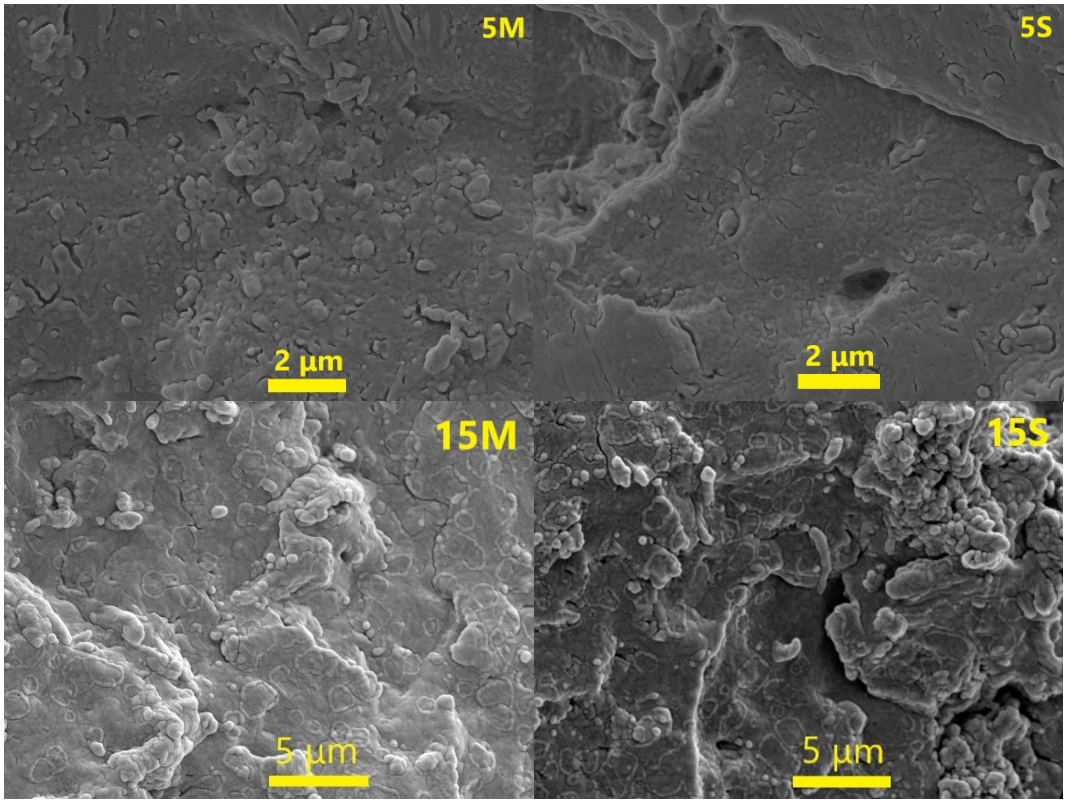

Fig. 3.13. SEM micrographs of selected compositions obtained by a fracture in liquid nitrogen.

Thermal properties

The effect of NFC filler loading on the thermal properties was investigated through differential calorimetric (DSC) analysis. The results are reported in Figs. 3.14 (a) and (b) and summarized in Table 3.7. The DSC second heating scan (Fig. 3.14 (a)) clearly shows a single peak. It indicates a slight increase in melting temperature (T_m), which can be attributed to thermal lag owing to the NFC filler's low thermal conductivity. The nanocomposites' crystallization behavior indicates an increase in crystallization temperature (T_c) and crystallinity (χ_c). The NFC promotes crystallization and acts as a nucleating agent indicated by an increase in crystallization temperature by 3 to 4 °C. Rastogi et al. reported similar observations for polyhydroxybutyrate/NFC composites [85]. Crystallinity was calculated from crystallization enthalpy instead of melt enthalpy, as it has been reported before that the melting process of PBS involves recrystallization [86]. Compared to neat PBS crystallinity 66 %, nanocomposites saw a slight crystallinity decrease to 54–58 % due to the obstructed PBS chain movements in the cooling process by the NFC filler presence. Melt blended samples show lower crystallinity than

solvent cast ones, and as seen in the structural analysis (SEM), filler dispersion is the main difference between the two preparation methods. Thus, an even spread filler interferes more with the crystallization process. However, it can also be concluded that the NFC samples can form a new crystalline polymer phase, which is consistent with the reported observation in literature for PLA/NC composites [87]. The increase in NFC filler up to 15 % loading slightly lowers the crystallinity.

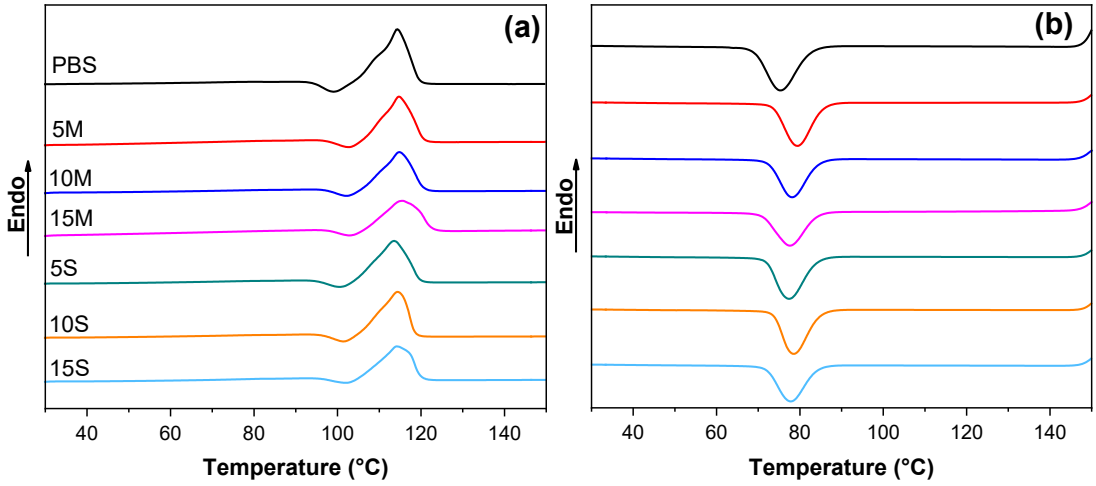

Fig. 3.14. DSC (a) heating curves and (b) cooling curves of PBS and 5, 10 and 15 wt.% PBS/NFC nanocomposites fabricated using the solution casting and melt compounding methods.

Table 3.7

Thermal Properties of PBS/NFC Composites

Sample	T_c, °C	ΔH_c, J/g	χ_c, %	T_m, °C	ΔH_m, J/g	$T_{5\%}$, °C	$T_{50\%}$, °C	T_{max}, °C	T_e, °C
PBS	75.0	72.9	66.0	114	75.1	357	401	404	571
5M	79.4	60.7	57.8	115	61.7	344	386	400	577
5S	77.4	60.0	57.2	114	53.1	337	382	396	577
10M	78.1	54.6	54.9	115	54.6	330	396	395	582
10S	78.5	58.1	58.4	114	59.3	338	387	400	561
15M	77.6	50.3	53.6	116	49.2	326	392	398	579
15S	77.8	54.1	57.6	114	50.9	308	389	398	583

Thermal degradation

The thermogravimetric analysis curves of neat PBS and nanocomposites are shown in Fig. 3.15. Table 3.7 presents an overview of thermal stability parameters $T_{5\%}$, $T_{50\%}$, which indicate the weight loss at 5 wt.% and 50 wt.%, correspondingly, while T_{max} and T_e show the maximum decomposition temperature and the ending decomposition temperature. A weight loss occurs faster for solvent cast samples above 120 °C losing 2–3 wt.%, which can be attributed to the remaining solvents in the composites. In contrast, the melt-processed samples and pristine PBS only saw a decrease in weight after 250 °C. $T_{5\%}$ of the nanocomposites indicates a difference in

decomposition temperature from 13 up to 49 °C compared to neat PBS. The decrease has been observed much more rapid for the solvent cast samples and samples with higher NFC filler sample concentration, indeed, as the region above 300 °C is the typical decomposition temperature for cellulose [88]. The maximum decomposition temperatures and $T_{50\%}$ for the nanocomposites were within the region of 5 °C, which also contained a 10 °C difference from PBS. As seen from the measurements, the overall thermal stability was decreased by 10 °C to 30 °C approximately compared to neat PBS, except for the 15S sample. The decomposition ended at around 570 °C, where the PBS's remaining mass was around 0.07 wt.%, while the nanocomposites remained around 1 wt.%, as there were no organic remains left it can be possibly attributed to inorganic char. The addition of NFC did not significantly impact the nanocomposites' application prospects, while relatively high decomposition above 250 °C indicates that recycling remains as a possibility.

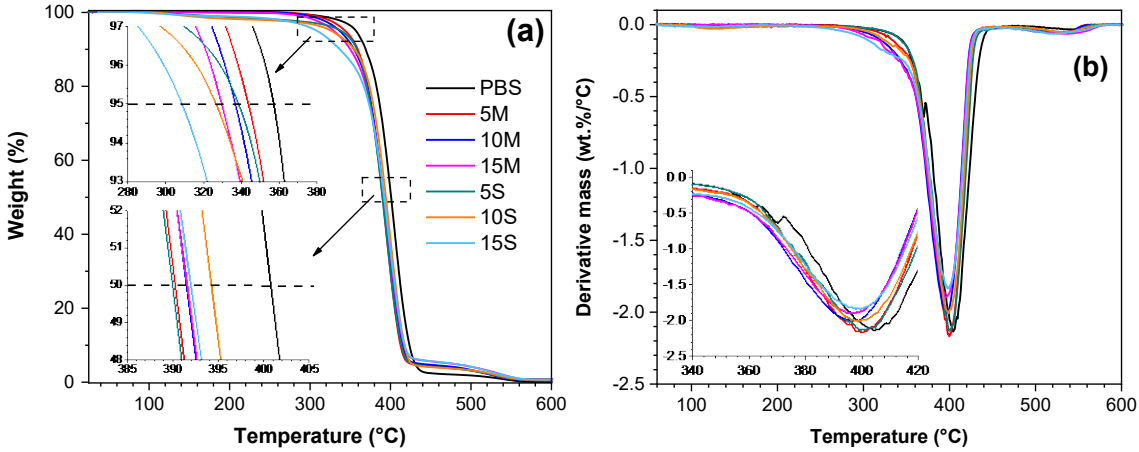

Fig. 3.15. (a) TGA thermogram and (b) first derivative TGA curves of PBS and (5, 10 and 15) wt.% PBS/NFC nanocomposites fabricated using the solution casting and melt compounding methods.

Biodegradation studies in the composting conditions

Visual and mass changes

Visual changes of PBS and nanocomposites during the biodegradation process are presented in Fig. 3.16. Five parallel samples for each specimen were used, and two of each were removed every 10 days to register changes. Nanocomposites can be distinguished by the light brown color caused by the thermal treatment of cellulose during the preparation process, which intensifies higher NFC loading for the composites. After 10 days, changes are minimal, but small dark spots where soil particles are embedded in the surface are visible, which after 10 more days have resulted in brown discoloration spots indicating degradation on the surface. Most notable changes after 20 days are visible for the 15M specimen, which has visible macro-scale holes that slowly appear for all nanocomposites at the 30- and 40-day mark.

In comparison, the PBS sample developed dark brown spots only between 30 and 40 days and visible holes after 60 days. This indicates that cellulose filler accelerates the biodegradation process. As this process is commonly known as hydrolysis, we believe that the hydrophilic and hydrophobic nature of cellulose and PBS influences the water adsorption speed. Thus, once the

top layer of PBS is breached, the matrix does not fully cover cellulose particles. They become local spots for more intensive biodegradation that involves the participation of microorganisms. From day 30 to day 50, nanocomposites lose their ductility and become fragile and fully discolored. Small cracks are visible, and a notable surface roughness increase can be seen. The color changes could be linked with the amorphous phase's degradation, which leads to crystallinity changes, as seen in Table 3.6. Finally, reaching the 70th day, nanocomposites become inseparable from the soil, very thin and extremely fragile. Almost no distinguishable nanocomposites particles could be recovered after 90 days. Although the PBS specimen was degrading slower and visually looked more intact, the film was thin and fragile and crumbled in small pieces, almost inseparable from the soil after the 80th mark. The mass changes were relatively linear after the initial 20 days and saw a slight increase with every 10 days until most of the samples were degraded at around the 60th day, where we saw a decrease in weight loss speed, which was partly impacted by the inability to separate the soil from specimens, thus contributing to measured mass. The mass changes clearly show that composites with higher cellulose content degrade faster.

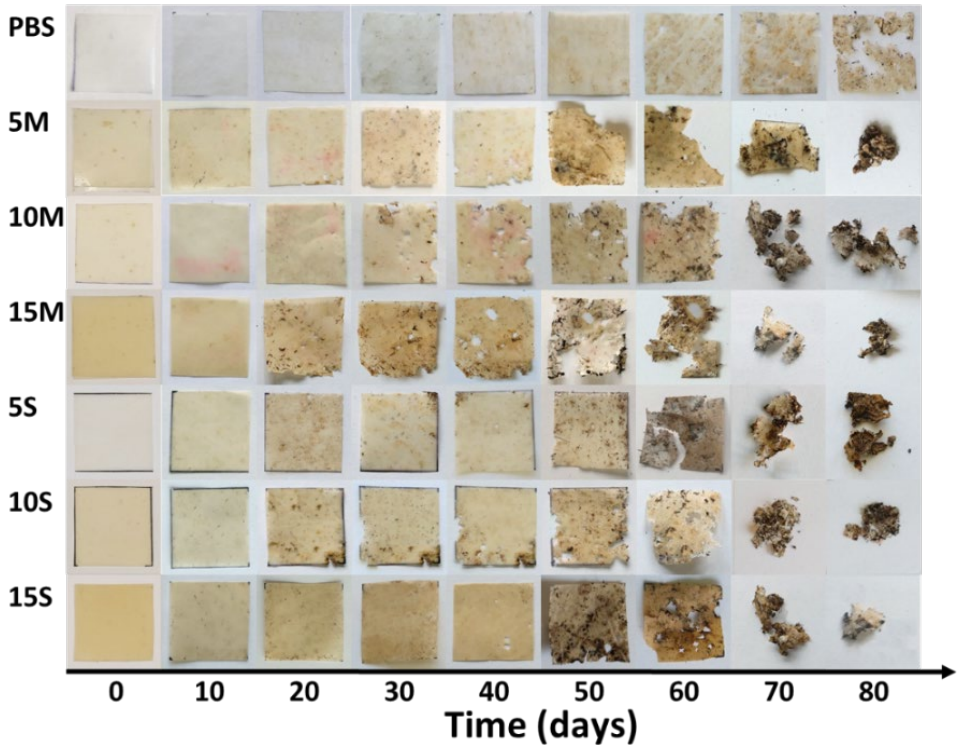

Fig. 3.16. Photos of biocomposite films during biodegradation process taken every 10 days until disintegration in the compost soil.

Mechanical properties

Tensile characteristics

The tensile modulus, ultimate strength, and elongation at break for the neat PBS and PBS /NFC nanocomposites are shown in Fig. 3.17 (a), (b). Also, stress-strain graphs for the selected samples are shown in Fig. 3.17 (d). The differences of neat PBS treatment did not reveal any notable changes. Because of the high intrinsic modulus of NFC, it acts as rigid reinforcement to the polymer matrix. The high aspect ratio of the NFC results in a large surface area for the

interaction with PBS matrix; thus, two limiting factors can be considered, the effective loading at which properties peak and adhesion between polymer and matrix. The composites' elastic modulus grew progressively with increasing NFC content for melt compounded samples showing a 1.4-fold and 1.7-fold increase for 5 % and 15 % samples, correspondingly. However, the solvent cast samples showed an almost 1.4-fold increase with higher NFC loadings (Fig. 3.17 (a)). Figure 3.17 (b) shows the composite's tensile strength indicating around a 10 % decrease compared to neat PBS, while most samples show similar values within margin error.

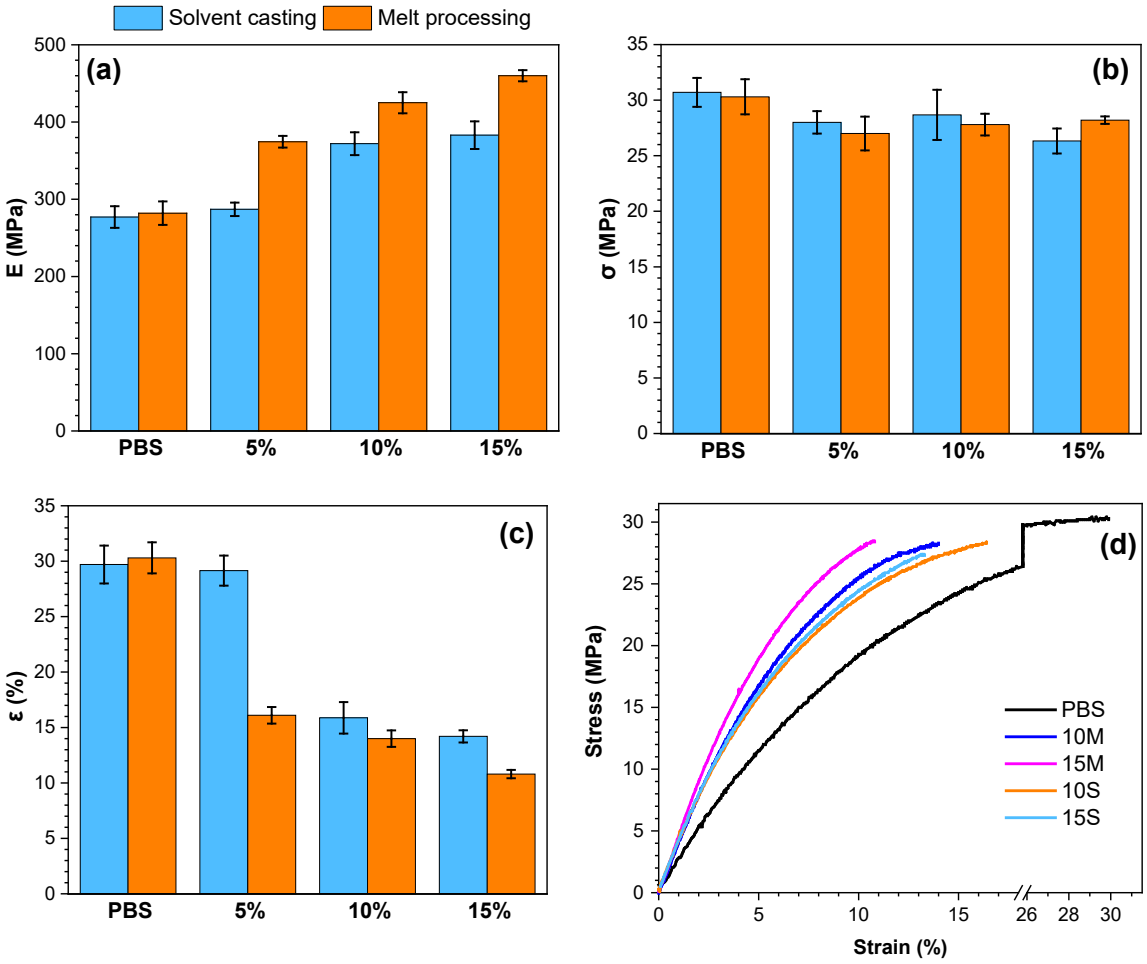

Fig. 3.17. Tensile properties: (a) tensile modulus; (b) tensile strength; and (c) elongation at break for PBS and 5, 10 and 15 wt.% PBS/NFC nanocomposites fabricated using solution casting and melt compounding methods. (d) Typical stress-strain curves presenting a ductile fracture in samples PBS, 10M, 15M, 10S, and 15S.

A slight reduction can be explained by limited adhesion between the filler and matrix, which has been observed for PBS [89] and other polyester polymers like PLA [90]. The NFC filler cannot properly support stresses transferred from the polymer matrix. Elongation at break shown in Fig. 17 (c) decreased with the increase of NFC content except for the 5S sample. The decrease in elongation values was around two-fold for most samples, while 15M had a 3-fold decrease. Melt compounded samples show an almost linear increase of modulus and linear decrease in elongation values indicating good ability to scale with NFC filler content; thus, a more homogeneous filler distribution is achieved.

Thermomechanical characteristics

Storage modulus E', loss modulus E'', and tan δ of neat PBS and nanocomposites are shown in Figs. 3.18 (a)–(c) as a function of temperature. Storage modulus values decreased with an increase in temperature as it is commonly observed for the polymers and sharply decreased in the glass transition region from –40 °C to +10 °C. NFC filler contributed to the material's high dimensional stability by significantly elevating values in all measured temperature ranges. The only notable exception was the 5S sample, which failed to form a reinforcement network; thus, agglomerates could not contribute to the stiffness of the composite in the viscoelastic state. The gradual increase of storage modulus values was observed with increased NFC concertation. At the same time, the melt blended samples showed higher overall values when filler loading was equally dispersed. The drastic increase of storage modulus for 15M composite compared to 5M and 10M, which performed similarly, could be explained by NFC's ability to form a continuous filler network in high loadings instead of separate particle reinforcement [91]. The highest storage modulus values were measured for 15M sample with the 1.4-fold increase at –70 °C and 2-fold increase at +70 °C compared to neat PBS. NFC hindered the polymer chains' movement, resulting in increased dampening properties, as shown in Fig. 3.18 (b). The increase in loss modulus values for all measured temperature ranges was observed for NFC loadings 10 and 15 wt.%. From –70 °C up to the glass transition, 15M showed the highest increase in loss modulus but was overtaken by 15S in the viscoelastic region.

The increase of loss modulus values can be explained by a decrease in crystallinity, which changes the required energy for the segmental movements of PBS [92]. Tan δ values show the ratio between storage and loss modulus, which decreases due to introduction of stiff nanoparticles into the polymer matrix, resulting in a reduced potential for energy dissipation and more elastic properties of nanocomposites than of neat PBS. The glass transition temperature can be determined from the tan δ peak in Fig. 3.18 (c). A clear shift to lower temperatures can be observed for all nanocomposites; for example, a sample with 15% of NFC shows the glass transition at –16 °C. Besides, the neat PBS has a glass transition at –21 °C. Owing to these changes, the interaction between filler and matrix can be an explanation. Another common explanation is the restricted chain mobility that impacts the segment rearrangement during the phase transition [93].

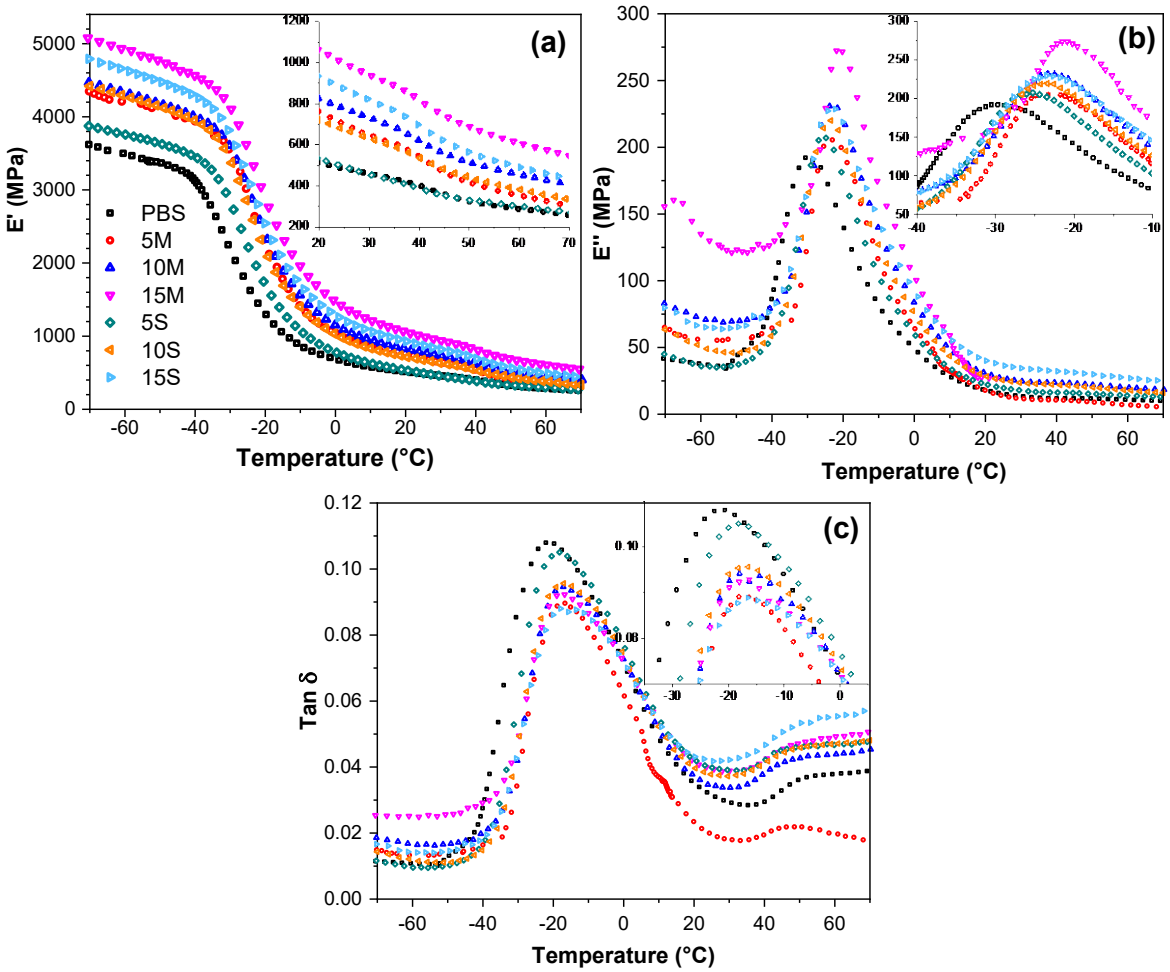

Fig. 3.18. Temperature dependence of (a) storage modulus, (b) loss modulus, and (c) tan δ curves from DMA measurements comparing PBS and 5, 10 and 15 wt.% PBS/NFC nanocomposites fabricated using the solution casting and melt compounding methods.

Summary

Nanofibrillated cellulose was used as a filler for poly(butylene succinate). Highly loaded 50 wt.% masterbatch preparation route was compared to conventional solvent casting. Based on the experimental results, the following conclusions are presented:

1. The mechanical properties increased with NFC loading, elastic modulus up to almost 1.7-fold, storage modulus up to 2-fold, and loss modulus up to 1.3-fold at room temperature. The masterbatch compositions had significantly higher values.
2. SEM analysis indicated good filler dispersion even at a high loading of 15 wt.% for the samples prepared from masterbatch, but solvent cast samples had visible agglomeration.
3. All composites degrade in composting conditions within 80 days.
4. The highly loaded masterbatch process has great potential for application in industrial composite film preparation for packaging and other applications. The composites gain increased stiffness, improved biodegradability, and, as described in the literature, increased barrier properties.

3.4. Highly loaded cellulose/poly(butylene succinate) sustainable composites for woody-like advanced materials application

Material processing and composite formulations

PBS was mixed with 70 % (w/w) cellulose in a thermo-kinetic mixer (Plastograph EC plus 50EHT, Brabender GmbH & Co. KG, Duisburg, Germany). Considering the previous investigations, which showed the possibility of high loadings of cellulose filler for PBS composites manufacturing, the MCC filler content was proposed to be equal to 70 wt.%. The processing temperature was set at 130 °C, and the screw speed was 70 rpm. In total, 40 g per batch were introduced in the thermo-kinetic mixer for a total mixing time of 7 min. The PBS and MCC were dried in a vacuum chamber at 40 °C for 24 hours before composite preparation.

The PBS/MCC composites were ground and compression-moulded with the Carver CH 4386 hydraulic press to obtain thin films. The plate temperature was set at 140 °C, and the material was preheated for 2 min and formed with a pressure of 3 metric tons for 3 min, followed by rapid cooling between metal plates at room temperature for 3 min. The dog-bone shape and stripes specimens were cut. These specimens were further tested for tensile, structural, dynamic-mechanical, density, calorimetric, and thermal properties.

Chemical modification of PBS/MCC composites

It is well known that the modification of the polymer/cellulose composites is needed to enhance the polymer and cellulose components' interface compatibility as a means to obtain high exploitation properties of the final composite material [27]. The strong interfacial adhesion and efficient stress transfer across phases of the polymer matrix and cellulose filler can be established by different modification additives during the composite processing. Based on this principle, the additives of MAH, PMDI, CDI, EST, PHA, APTMS are used to adjust the interfacial interactions through compatibilization of the components [78]–[85]. The used compositions and the modification procedures were selected regarding the literature data and preliminary tryouts. Altogether, seven different PBS/MCC compositions were obtained by using different chemical modification treatments of composites to improve the compatibility between the components (Table 3.8). The obtained PBS/MCC composites and specimens were stored in sealed bags before any testing.

Table 3.8

Obtained PBS/MCC Compositions

Sample	Description of modification
PBS	Neat polymer
70MCC	Untreated microcrystalline cellulose
70MAH	Maleic acid anhydride
70PMDI	Polymeric diphenylmethane diisocyanate
70CDI	Carbodiimide
70EST	Aliphatic ester
70PHA	Polyhydroxyamide
70APTMS	(3-Aminopropyl) trimethoxysilane

For PBS/MCC composite modification, 1 wt.% of MAH, 1.5 wt.% of PMDI and 3 wt.% of CDI were loaded during the melt processing process with a thermo-kinetic mixer [81]–[84]. At the same time, the modified MCC was blended with PBS without any additional additive loading. The modified MCC preparation was done as follows: 30 g of MCC was suspended in 500 ml water, and the mixture was homogenized with ultrasound sonification for 10 minutes. Slowly 90 ml of PHA or EST were added in 2 hours, stirring and ultrasound sonification were applied sequentially for 30 min time periods [85]. The acquired modified MCC suspensions were then filtrated and dried in a vacuum. For the salinization, 50 mL of APTMS was dissolved in 250 mL distilled water and stirred, while the solution pH was stabilized to 4 by the addition of acetic acid [52]. 50 g MCC was added to the solution after pH was fixed at 4. The mixture was stirred at room temperature for 2 h followed by filtration and drying in a vacuum. Chemical reaction and permanent surface modification of MCC accomplished a vacuum oven at 120 °C for 2 h.

Thermal properties

TGA was used to investigate the influence of the composition on the thermal sensitivity and degradation properties of PBS/MCC composite materials. Figure 3.19 showed TGA (a) and DTG (b) curves of PBS/MCC composites. All PBS/MCC compositions showed a small mass loss of 2 % below 100 °C, corresponding mainly to the removal of residual water [28]. The degradation mechanism and degradation temperature of neat PBS and PBS/MCC composites differed strongly. It is assumed that MCC has lower thermal stability than neat PBS polymer [29], [30]. This means that the incorporation of the MCC induced less thermal stability of PBS/MCC composites. Lee et al. reported this for PBS/kenaf fiber composites [31]. The temperature at 5 % mass loss for the 70MAH composition was 240 °C and for 70EST composition it was 290 °C. The rest of the composites showed a 5 % mass loss in the temperature range of approximately 240–290 °C. The PBS exhibited only single-stage degradation with a peak at 406 °C, whereas MCC filled composites revealed two degradation peaks in the temperature range of 301–398 °C. It indicated that the single-stage thermal degradation process was defined primarily by the PBS polymer chain degradation, while PBS/MCC composites degradation was affected by cellulose incorporation, mutual interaction between polymer matrix and fillers, and filler surface modification. Roman and Winter evidenced the strict relation of cellulose surface modification and its thermal stability [32]. The temperature at 50 % mass loss for PBS was 401 °C. The first stage of degradation in DTG (Fig. 3.19 (b)) is at around 310 °C for the MCC sample; while for 70MAH, 70PMDI, and 70CDI composites the thermal degradation shifted to lower temperature, 315 °C, then for 70EST, 70PHA, and 70APTMS composites, thermal stability increased up to 340 °C. The composites loaded with chemically coupled and modified MCC revealed enhanced thermal degradation temperature at 50 % mass loss up to 360 °C. This was described to the formation of crosslinked structures with the altered chains and inhibited chain release during the formation of the char in the thermal degradation process [33]. The similar behavior of thermally more stable PBS composite than neat PBS was reported by Tang et al. [34] when using grafted-nanocellulose as reinforcement.

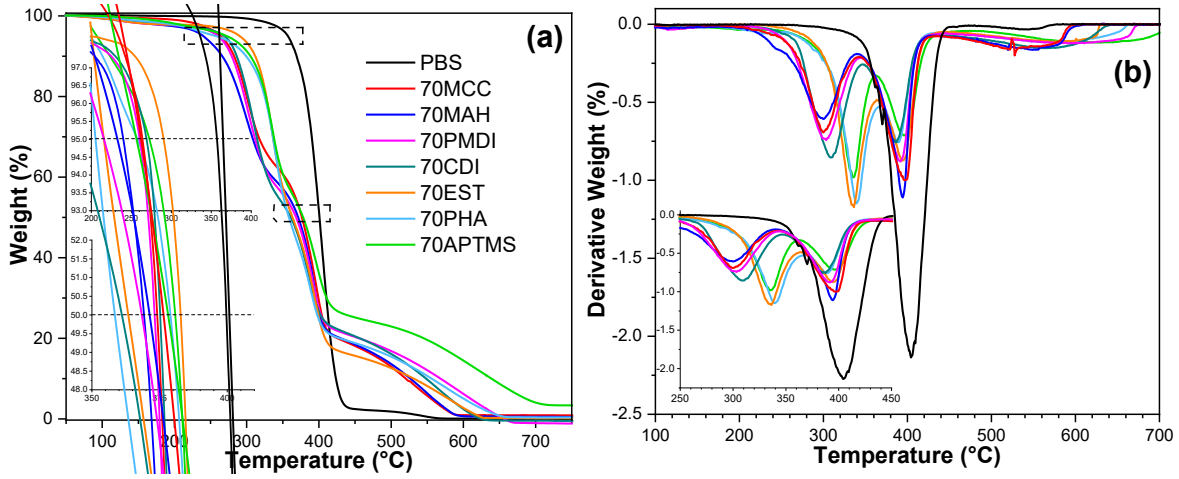

Fig. 3.19. (a) TGA curves and (b) DTG of PBS/MCC composites.

The results of DSC in the form of the heating and cooling thermal curves of PBS/MCC composites are shown in Fig. 3.20. The thermal curves showed a characteristic endothermic melting transition (Fig. 3.20 (a)) and exothermic crystallization transition (Fig. 3.20 (b)). In Table 3.9, the experimental values of melt temperature (T_m), crystallization temperature (T_c), enthalpy of melting (H_m), enthalpy of crystallization (H_c), crystallinity (χ), density (d), and voids (Δ) are presented. All samples with modified MCC showed a very pronounced decrease in X compared to neat PBS and also in comparison to the 70MCC sample. The X of neat PBS has been found to be about 68 %. In the case of 70APTMS, 70PHA and 70EST samples χ has decreased to 52, 56, and 58 % correspondingly. Similar findings have also been also reported in the literature [38]. The MCC's silane treatment improved its dispersion in a polymer matrix, reduced agglomeration, and suppressed the crystalline phase more strongly than PHA and EST modifications of MCC filler [39]. The chain cross-linking and/or extension mechanisms can even further limit polymer chain movements and reduce crystallinity [35]. It is observed that crystallinity decreased by about 20 % for compositions 70MAH, 70PMDI, and 70CDI in comparison to neat PBS. Melting temperature T_m and crystallization temperature T_c of the obtained samples was modestly decreased and increased correspondingly. This means that

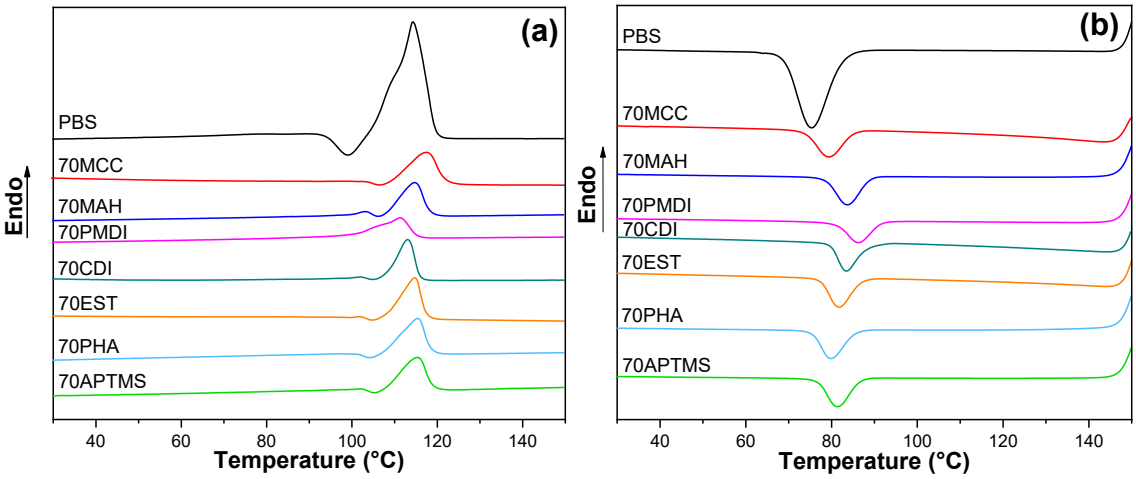

Fig. 3.20. DSC curves of PBS/MCC composites: (a) heating, (b) cooling.

crystallization of polymer chains with altered flexibility and mobility in the composites interfered with the crystallization process [34], [36], [38], which has started earlier at higher temperatures and resulted in lower crystallinity by about 30 % of the final composite.

Structure and morphology characterization

Experimental density values d of the composites, obtained by the weighting method [40], are summarized in Table 3.9. The value of parameter *d**, defined as the apparent density of the polymer, was calculated by the equation reported in [41]. It can correspond to the decrease of the polymer density due to the pronounced drop in crystallinity observed in DSC. SEM images of the fractured surfaces of PBS/MCC composites (Fig. 3.21) evidenced the aggregates of MCC particles. According to the literature [42], [43], cellulose particles had a common tendency to aggregate at high MCC loadings. The fractured surfaces of the 70MCC sample were very rough. MCC particles can be seen for 70MCC, 70MAH, 70EST, and 70PHA samples. In turn, the surfaces of samples 70CDI, 70PMDI, and 70APTMS looked smooth, homogeneous, and dense in different magnifications.

The characteristic groups of the composites can be evaluated by FTIR spectroscopy. The representative FTIR spectra of the tested compositions are shown in Fig. 3.22, and selected spectra overlays in Fig. 3.23. The characteristic absorption peaks associated with components are highlighted. The absorption band between 3600 cm^{-1} and 3100 cm^{-1} (1) corresponds to OH vibration in MCC. The band between 3000 and 2800 cm^{-1} with the absorption band at 2946 cm^{-1} (2) and the band at 1331 cm^{-1} (4) corresponds to symmetric and asymmetric CH_2 stretching vibration [47]. While 1712 cm^{-1} (3) C=O stretching vibrations of the ester group are usually used as one of the key bands to characterize PBS spectra [19], [48]–[50]. The band at 1150 cm^{-1} (5) is an absorption band for the C-O stretching vibration of PBS. The decrease in its intensity reflects a reduction in the crystallinity of the composite material [49]. A shift of this band corresponds to the interaction between cellulose and polymer chain in the composite [51]. Finally, a band between 1050 and 1010 cm^{-1} with the maximum at 1046 cm^{-1} (6) corresponds to the stretching vibration of the O-C-C. In the 70APTMS sample's spectra, a new absorption band is observed at 1557 cm^{-1} and has been attributed to the NH scissoring bending vibration [48], [50], [52]. In the 70EST sample's spectra, there are decreased intensities of the ester's C=O and C-O characteristic bands at 1712 cm^{-1} and 1150 cm^{-1}, correspondingly, while the intensity of O-C-C group's band increased at 1046 cm^{-1}. This could indicate the intramolecular interactions between the ester chains and the cellulose surface. An absorption band at 1100 cm-1 could be attributed to C-O stretching vibration for the aliphatic ether linkage in the interphase of cellulose and polymer matrix. In the 70PHA sample, there is a noticeable increase of the ester's group bands intensities at 1712 cm^{-1} and 1150 cm^{-1} that could have resulted from the ester linkages formed between the cellulose and polymer. In turn, the 70CDI composition can be characterized with the new bands at 1556 cm^{-1} and 1245 cm^{-1} that could correspond to the NH and CN, correspondingly [53]. The reaction of the carbodiimides and the end-groups of carboxyl groups of the polyester macromolecules could lead to the chain extension, chain crosslinking, and the formation of the urea group linkages. The 70PMDI spectra has shown absorption bands at 1603 and1510 cm^{-1}, which could be attributed to the C=O urethane group stretching and C=C aromatic rings, correspondingly; these linkages could

be formed between the isocyanate and the hydroxyl groups on cellulose, and the isocyanate and the carboxylic acid end-groups of the polyester [45], [54], [55].

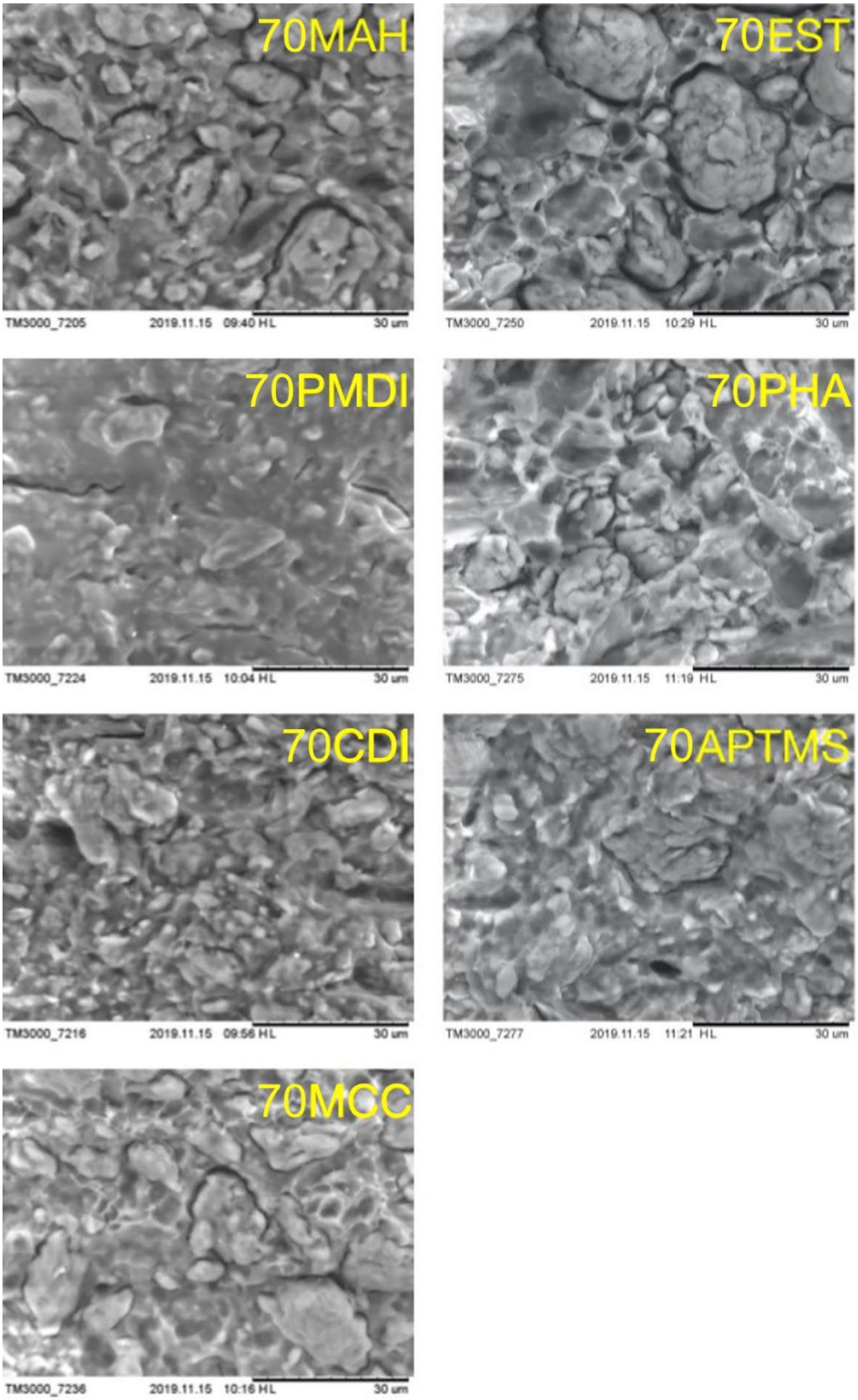

Fig. 3.21. SEM micrographs of fractured surfaces of PBS/MCC composites.

The 70MAH composition is characterized by the characteristic absorption bands at 1712 cm^{-1} and 1150 cm^{-1}, which can testify the formation of the ester linkages between the maleic anhydride and the hydroxyl groups of the cellulose [44].

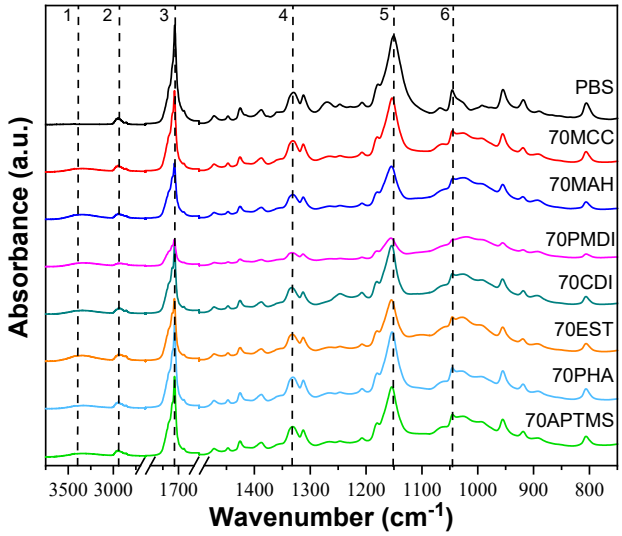

Fig. 3.22. FTIR spectra of PBS/MCC composites.

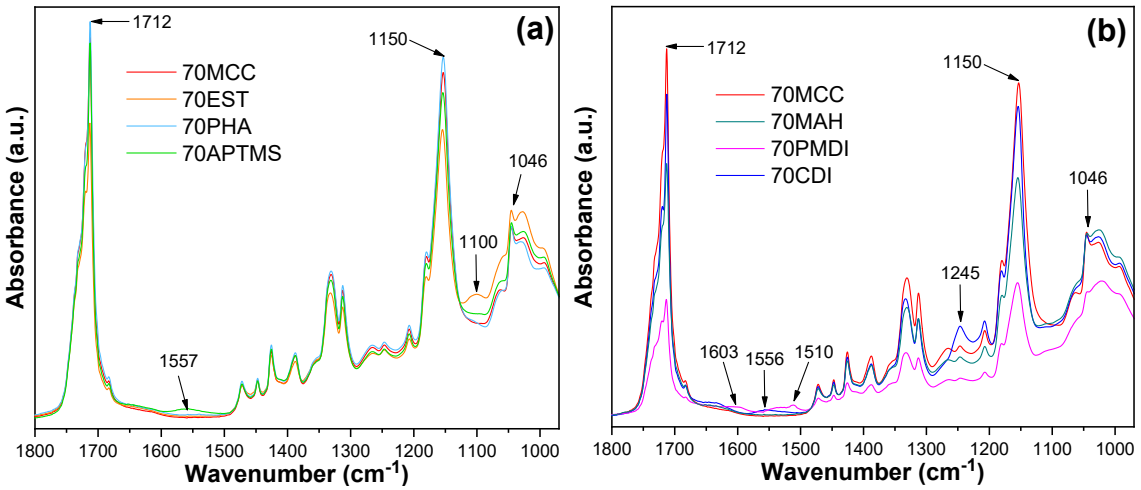

Fig. 3.23. FTIR spectra of PBS/MCC composites with spectra overlays.

Thermomechanical properties

The dynamic mechanical data of the composites were measured with respect to the temperature. The viscoelasticity of PBS/MCC composite improved and rigidity dropped with an increase of temperature. Figure 3.24 shows the temperature dependence of storage modulus *E'*, loss modulus E'', and damping factor tan δ for PBS/MCC composites. PBS has three regions in the DMA curve: glassy, glass transition, and rubbery. The glass transition region of PBS started with a sharp decrease in storage modulus that corresponded to the peak in loss modulus and tan δ graphs. The introduced 70 wt.% loading of MCC into PBS polymer can restrict overall chain mobility severely that drastically raises its viscosity [56], [57]. Accordingly, MCC composites showed a less pronounced transition between the glassy and rubbery states. The modified compositions characterized the improved stiffness after the PHA, CDI, PMDI, and

APTMS treatment due to the efficient cross-linking and chain extending of the composite and polymer, correspondingly [35]. The limited polymer chain flexibility leads to a strong increase in material viscoelasticity. Furthermore, the *E′* and *E*'' increased in all temperature range for those samples. For example, there was an almost 4-fold increase in *E′* for the 70APTMS composition at room temperature in comparison to neat PBS. The APTMS treatment provided an almost 1.6-fold increase at +70 °C and a 2-fold increase at 0 °C in *E′* in comparison to the 70MCC sample. In contrast, the 70PMDI treatment gave 2.5-fold at +70 °C and 1.7-fold increase at 0 °C. In turn, the EST composition showed a pronounced enhancement in viscoelasticity properties and a decrease in stiffness compared to 70MCC, which can be related to plasticization of the material by introducing the long alkyl chains of the ester surfactant molecules [61]. It also showed strong enhancements in *E*'', which testified that higher energy was demanded for the polymer viscoelastic deformation [62].

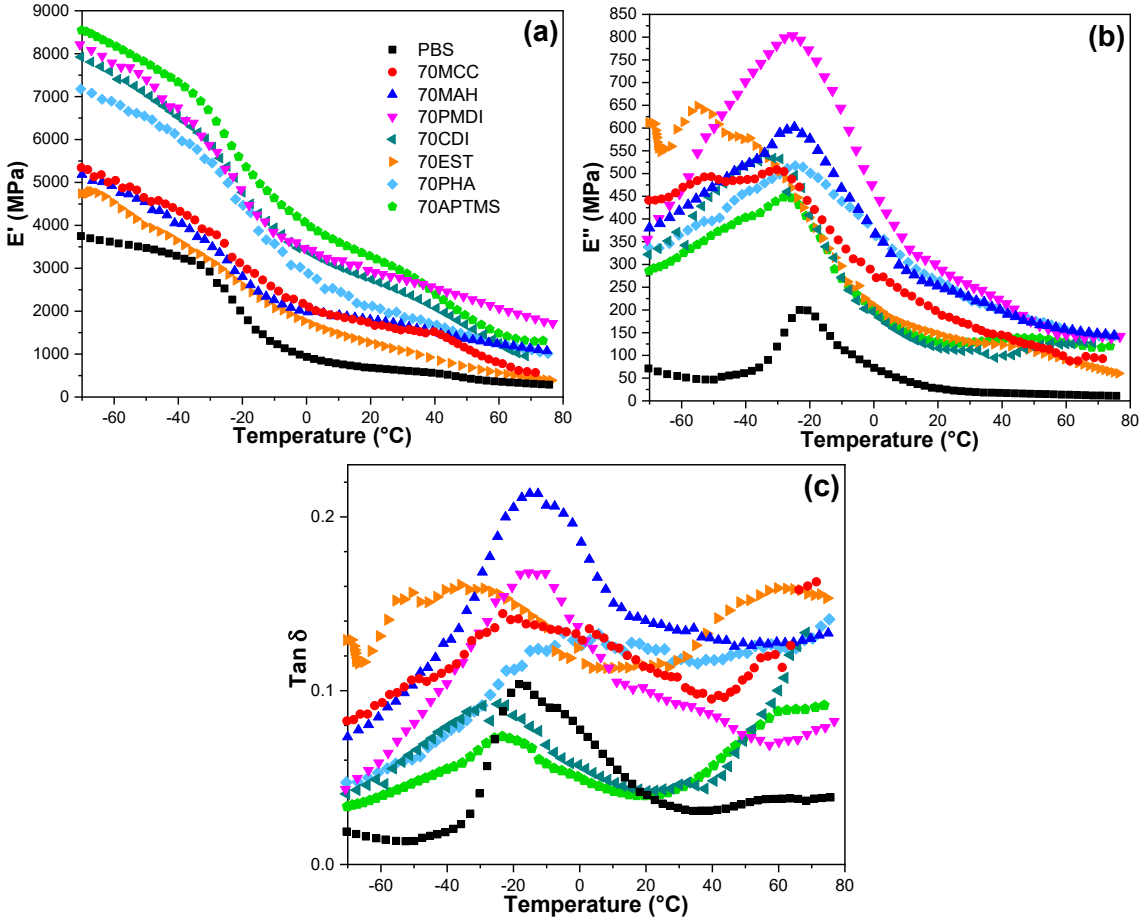

Fig. 3.24. DMA curves of PBS/MCC samples: (a) storage modulus *E*'; (b) loss modulus *E*''; and (c) loss factor tan δ.

Mechanical properties

The tensile properties of the PBS/MCC composites were tested in tension mode. The Young's modulus E increased almost 4.5-fold for the 70MCC composite in comparison to neat polymer (Fig. 3.25 (a)). As expected, the additional cross-linking treatment of MCC composites increased the compatibility of the cellulose filler and the polymer matrix. As a result, the E values are increased to some extent. E values of the 70PMDI, 70CDI and 70APTMS

compositions were remarkably higher than for the 70MCC composite, which means the improving of the compatibility, stress transfer efficiency and the interfacial strength through the establishment of chemical bonds at the interfaces between cellulose and polymer matrix phases [27]. The E value raised 1.4-fold for 70PMDI, 1.6-fold for 70CDI, and 1.1-fold for 70APTMS, correspondingly. The tensile strength σ values for those samples were also significantly higher than for the 70MCC composition and similar to the initial neat PBS. The obtained σ values and the E values of the modified MCC composites are comparable to the polymer/wood composites reported by several authors [44], [65], [70].

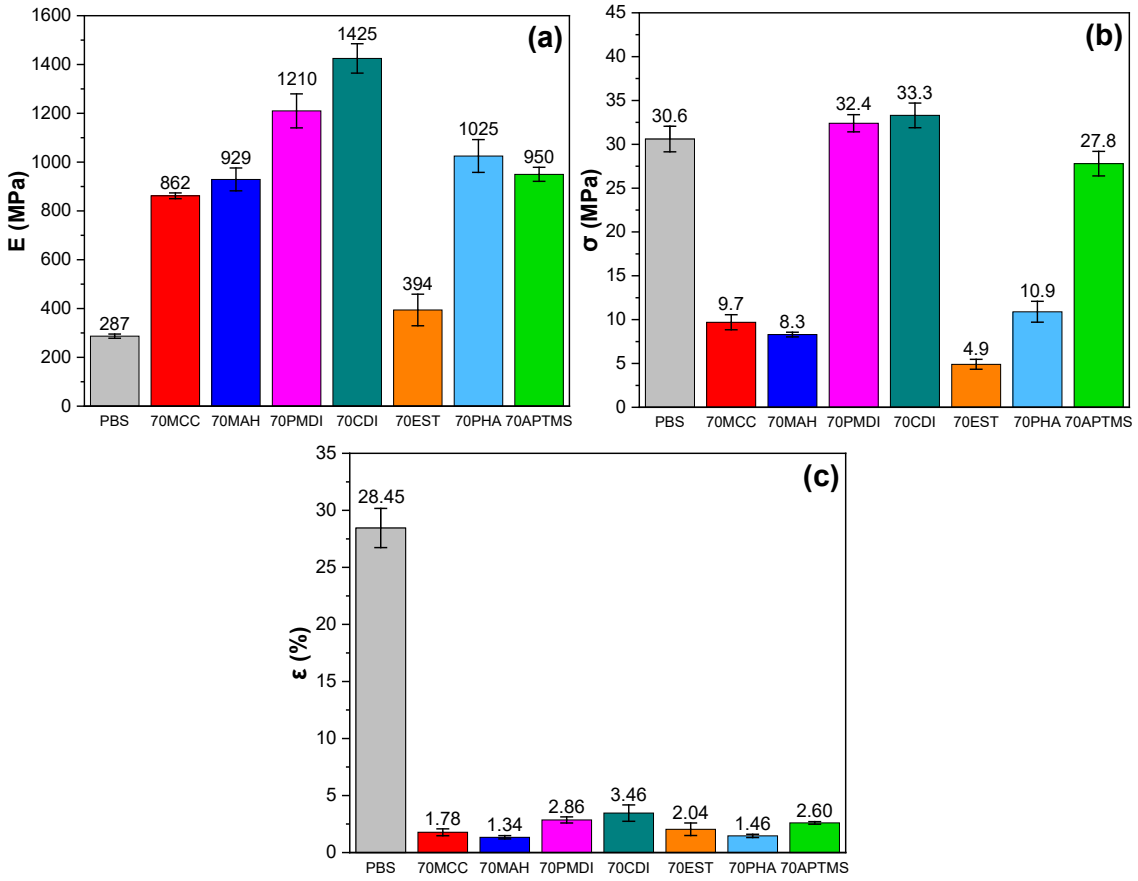

Fig. 3.25. Tensile properties for PBS/MCC composites: (a) elastic modulus *E*; (b) strength σ; and (c) strain ε.

Table 3.9

Thermal and Physical Characteristics of PBS/MCC Composites

Sample	T_m, °C	T_c, °C	H_m, J/g	H_c, J/g	χ_c, %	d, g/cm^3	d*, g/cm^3
PBS	114.2	75.3	75.1	72.9	68.0	1.365	-
70MCC	117.5	79.4	21.4	19.8	64.6	1.370	0.947
70MAH	114.7	83.6	16.9	20.4	51.0	1.362	0.925
70PMDI	111.3	86.2	15.8	16.0	47.6	1.336	0.851
70CDI	113.1	83.4	15.6	16.8	47.1	1.315	0.791
70EST	114.8	81.8	19.2	18.2	57.9	1.385	0.990
70PHA	115.3	80.0	18.5	20.3	55.8	1.402	1.038
70APTMS	115.2	81.3	17.3	20.2	52.2	1.385	0.990

*calculated using the MCC density = 1.600 g/cm^3 [64].

Biodegradation under composting conditions

The obtained biocomposites modified by different chemical routes showed further degradation, indeed, only after 30 days in compost soil. The biodegradation of the biocomposites was maintained until the complete disintegration of the material or up to 90 days, as shown in Fig. 3.26. The received results reveal that the cellulose and polymer modification chemistry significantly impact biocomposites.

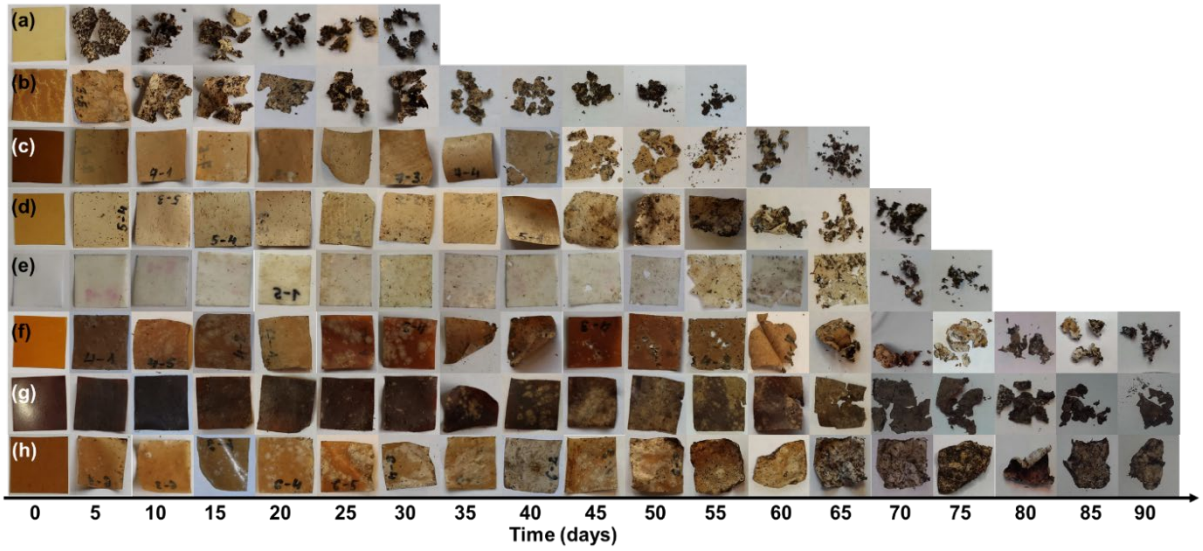

Fig. 3.26. Biocomposites degradation in composting conditions: (a) 70EST, (b) 70MAH, (c) 70PHA, (d) 70MCC, (e) PBS, (f) 70APTMS, (g) 70PMDI, (h) 70CDI.

PHA, APTMS, PMDI, and CDI treatment reduced composites biodegradation, which becomes even longer than for the neat PBS and 70MCC composite. This shows that surface wettability does not directly translate to accelerated degradation due to the developed good adhesion between the filler and matrix [94] and decreased surface area for the degradation process [95]. The behavior of biocomposites 70EST and 70MAH is opposite to the previous ones. 70EST and 70MAH degrade rapidly in 5 to 15 days and the samples cannot be separated from the soil as seen after 30 and 55 ageing days, correspondingly. The total biodegradation of the obtained biocomposites corresponds to that of polyesters PBS and biodegradable cellulose character promoted by its hydrolysis under high humidity and bacteria conditions [96], [97]. It has been reported that both low crystallinity of the polymer and high hydrophilicity of the cellulose facilitated the water wetting the composites surface, enhanced water penetration, and promoted the attack of water molecules on the polymer chains [98]. Chemically modified biocomposites with incorporated polar functional groups of amines and carbonyls can absorb moisture through hydrogen bonds, then biodegradation occurs rapidly [31]. While non-polar nature silane and urethane functional groups introduced into the chains slow down the sample's total deterioration to 90 days.

Summary

Six additives (MAH, PMDI, CDI, EST, PHA, and APTMS) were selected for compatibilization of highly loaded poly(butylene succinate) (PBS) and micro cellulose (MCC) composites. Based on the experimental results, the following conclusions are presented:

1. Tensile strength was enhanced around 3-fold for 70CDI, 70PMDI, and 70APTES compared to the unmodified composite (70MCC), while elastic modulus values were enhanced for all compositions (except 70EST) 1.1- to 1.7-fold. Similarly, thermomechanical properties had a significant increase in storage modulus values, up to a 6-fold increase at 75 ˚C for prepared modified composites compared to neat PBS.
2. SEM analysis indicated that the surface of 70CDI, 70PMDI, and 70APTMS samples looked smooth, homogeneous, and dense at different magnifications.
3. The 70EST composite degraded remarkably in 30 days, more than two times faster than neat PBS, while the 70CDI and 70PMDI samples retained at least a third of their mass after 90 days.
4. Modifications allow for highly tuneable composite properties, which, in turn, is excellent for adapting compositions for various applications.

4. COMPOSITE MATERIAL PROPERTIES – AN OVERVIEW

In total, the Thesis includes the preparation of 23 composites with a comparison to neat PBS. Table 4.1 summarizes the highest loadings of three cellulose fillers prepared in various ways and two of the best compatibilized compositions of MCC. From the obtained data, it is clear that the most significant changes are observable in mechanical and thermomechanical properties. Generally, the addition of cellulose fillers resulted in a stiffer material compared to PBS. The addition of cellulose fillers also increased the crystallization temperature and decreased the crystallinity. Crystallinity was significantly reduced as a result of the modifications. All cellulose fillers reduce the thermal stability of composites compared to neat PBS. However, the processing temperatures used for melt mixing at 130–160 °C are significantly lower than even the initial degradation that occurs above 250 °C. Modifications strongly shifted the glass transition temperature. But for the composites prepared only from cellulose and PBS, the melting and the glass transition temperatures remained close to the PBS value.

Table 4.1

Overview of Properties for Highly Loaded Composites for Representative Fillers and Preparation Methods.

Properties	PBS	50rCell	40MCC	40NFC	15S	15M	70MCC	70CDI	70APTMS
T_m, °C	114	115	117	114	114	116	118	113	115
T_c, °C	75	90	85	82	78	78	79	83	81
χ_c, %	66	14	64	53	58	54	65	47	52
$T_{50\%}$, °C	401	384	382	384	389	392	377	363	380
E, MPa	271	866	613	561	383	460	862	1425	950
σ, MPa	30.9	12.6	22.5	12.9	26.3	28.2	9.72	33.3	27.8
ε, %	33.3	1.99	5.11	3.18	14.2	10.8	1.78	3.46	2.60
E', MPa (20°C)	683	2001	1495	1395	931	1060	1731	2750	3274
E'', MPa (20°C)	27	139	58	53	40	27	198	116	129
T_g, °C	-18	-18	-16	-17	-16	-17	-21	-26	-23

The biodegradation time in days for prepared composites is shown in Table 4.2. The results indicate that cellulose accelerates the degradation of composites compared to neat PBS, but the use of various compatibilizers and chemical modifications can significantly shift the degradation time in both directions, i.e., shorter or longer. Furthermore, increasing the cellulose content reduces the time it takes for the composite to degrade.

Table 4.2

Comparison of Biodegradation Time

	PBS	PBS/rCell composites	PBS/MCC/NFC melt composites	PBS/NFC solution and masterbatch composites	PBS/70 wt.% MCC compatibilized composites
Biodegradation time in the composting conditions, days	75–85	70	65–70	80	30–90 (2 remained even after 90 days)

5. CONCLUSIONS

1. In total, 23 different types of compositions were prepared within the scope of the Tesis, with cellulose filler loading ranging from 5 to 70 wt.%. Three different types of cellulose fillers were successfully integrated into composite formulations – recycled cellulose, microcrystalline cellulose, and nanofibrillated cellulose. The compositions were studied using melt blending, masterbatch melt processing, and solution casting methods. Six different types of modification methods were tested, and their tuneable properties were determined.

2. The freeze-dried NFC powder direct melt incorporation into PBS resulted in agglomeration of cellulose filler and poor mechanical performance of the composite compared to the PBS/MCC composite. PBS/NFC composites prepared with the masterbatch process showed up to 30 % higher mechanical and thermomechanical properties at room temperature compared to those prepared with the solution method.

3. Chemical modifications of the MCC composites led to enhanced mechanical, thermo-mechanical, and thermal properties of the PBS/MCC composites. The high loading of 70 wt.% MCC demanded compatibilization between filler and matrix. Chemical modifications influenced the glass transition temperature – 10–20 °C shifts to both higher and lower temperatures. The modification of cellulose prior to melt mixing increased the thermal stability of the composite material by up to 30 °C.

4. Biodegradation under composting conditions showed that PBS degrades completely in 75 to 85 days, while the addition of cellulose accelerated biodegradation by approximately 10 days. Higher loadings of cellulose accelerated biodegradation, with the most notable difference observable at concentrations of 5 to 10 wt.%. The cellulose type only slightly influences degradation. Chemical modification strongly influenced the PBS/MCC composite biodegradation time, which ranged from 30 to 90 days with some compositions retaining part of their mass even after 90 days.

5. Biocomposites are suitable for a variety of applications, like WPCs, packaging materials, mulch films, and many more, and these composites only start to degrade when buried in the soil. The exceptional thermal stability exhibited by compositions during processing proved that PBS/cellulose composites are compatible with conventional processing methods and can be produced on an industrial scale.

REFERENCES

1. Xu, J.; Guo, B. H. Poly(butylene succinate) and its copolymers: research, development and industrialization. *Biotechnology Journal* **2010**, *5*, 1149–1163, doi:10.1002/biot.201000136.
2. BioPBS™FZ71PM Technical Data Sheet. Availabe online: http://www.pttmcc.com/new/download/BioPBS_FZ71PM_Technical_Data_Sheet_for_Extrusion_Coating1.pdf (accessed on 05.05.2021).
3. Biopolymers – facts and statistics. Availabe online: https://www.ifbb-hannover.de/en/facts-and-statistics.html (accessed on 23.03.2021).
4. Garside, M. Global plastic production 1950–2019. Availabe online: https://www.statista.com/statistics/282732/global-production-of-plastics-since-1950/ (accessed on 23.03.2021).
5. SDK to Terminate Production and Sale of Biodegradable Plastic. Availabe online: https://www.sdk.co.jp/english/news/15030/16250.html (accessed on 23.03.2021).
6. A Friendly Catalyst to help you become an environmentally friendlier brand. Availabe online: http://www.pttmcc.com/new/faq.php (accessed on 23.03.2021).
7. Polybutylene succinate resin. Availabe online: https://fillplas.com/polybutylene-succinate-pbs-fillplas-resin/ (accessed on 23.03.2021).
8. Rudnik, E. 10 - Compostable Polymer Materials: Definitions, Structures, and Methods of Preparation. In *Handbook of Biopolymers and Biodegradable Plastics*, Ebnesajjad, S., Ed. William Andrew Publishing: Boston, 2013, 189-211, doi:10.1016/B978-1-4557-2834-3.00010-0pp.
9. Patel, M. K.; Bechu, A.; Villegas, J. D.; Bergez-Lacoste, M.; Yeung, K.; Murphy, R.; Woods, J.; Mwabonje, O. N.; Ni, Y.; Patel, A. D., et al. Second-generation bio-based plastics are becoming a reality – Non-renewable energy and greenhouse gas (GHG) balance of succinic acid-based plastic end products made from lignocellulosic biomass. *Biofuels, Bioproducts and Biorefining* **2018**, *12*, 426–441, doi:10.1002/bbb.1849.
10. Wang, G. X.; Huang, D.; Ji, J. H.; Volker, C.; Wurm, F. R. Seawater-Degradable Polymers-Fighting the Marine Plastic Pollution. *Advanced Science* **2020**, *8*, 2001121, doi:10.1002/advs.202001121.
11. Kim, H.-S.; Yang, H.-S.; Kim, H.-J. Biodegradability and mechanical properties of agro-flour-filled polybutylene succinate biocomposites. *Journal of Applied Polymer Science* **2005**, *97*, 1513–1521, doi:10.1002/app.21905.
12. Liu, L.; Yu, J.; Cheng, L.; Yang, X. Biodegradability of poly(butylene succinate) (PBS) composite reinforced with jute fibre. *Polymer Degradation and Stability* **2009**, *94*, 90–94, doi:10.1016/j.polymdegradstab.2008.10.013.
13. Calabia, B.; Ninomiya, F.; Yagi, H.; Oishi, A.; Taguchi, K.; Kunioka, M.; Funabashi, M. Biodegradable Poly(butylene succinate) Composites Reinforced by Cotton Fiber with Silane Coupling Agent. *Polymers* **2013**, *5*, 128–141, doi:10.3390/polym5010128.
14. Zhao, J.-H.; Wang, X.-Q.; Zeng, J.; Yang, G.; Shi, F.-H.; Yan, Q. Biodegradation of poly(butylene succinate) in compost. *Journal of Applied Polymer Science* **2005**, *97*, 2273–2278, doi:10.1002/app.22009.
15. Cho, H. S.; Moon, H. S.; Kim, M.; Nam, K.; Kim, J. Y. Biodegradability and biodegradation rate of poly(caprolactone)-starch blend and poly(butylene succinate) biodegradable polymer under aerobic and anaerobic environment. *Waste Management* **2011**, *31*, 475–480, doi:10.1016/j.wasman.2010.10.029.
16. Kasuya, K.-I.; Takagi, K.-I.; Ishiwatari, S.-I.; Yoshida, Y.; Doi, Y. Biodegradabilities of various aliphatic polyesters in natural waters. *Polymer Degradation and Stability* **1998**, *59*, 327–332, doi:10.1016/S0141-3910(97)00155-9.

17. Nakayama, A.; Yamano, N.; Kawasaki, N. Biodegradation in seawater of aliphatic polyesters. *Polymer Degradation and Stability* **2019**, *166*, 290–299, doi:10.1016/j.polymdegradstab.2019.06.006.
18. Ferreira, F. V.; Dufresne, A.; Pinheiro, I. F.; Souza, D. H. S.; Gouveia, R. F.; Mei, L. H. I.; Lona, L. M. F. How do cellulose nanocrystals affect the overall properties of biodegradable polymer nanocomposites: A comprehensive review. *European Polymer Journal* **2018**, *108*, 274–285, doi:10.1016/j.eurpolymj.2018.08.045.
19. Kumari Pallathadka, P.; Koh, X. Q.; Khatta, A.; Luckachan, G. E.; Mittal, V. Characteristics of biodegradable poly(butylene succinate) nanocomposites with thermally reduced graphene nanosheets. *Polymer Composites* **2017**, *38*, E42-E48, doi:10.1002/pc.23824.
20. Lambert, S.; Wagner, M. Environmental performance of bio-based and biodegradable plastics: the road ahead. *Chemical Society Reviews* **2017**, *46*, 6855–6871, doi:10.1039/c7cs00149e.
21. Gigli, M.; Fabbri, M.; Lotti, N.; Gamberini, R.; Rimini, B.; Munari, A. Poly(butylene succinate)-based polyesters for biomedical applications: A review. *European Polymer Journal* **2016**, *75*, 431–460, doi:10.1016/j.eurpolymj.2016.01.016.
22. Veranitisagul, C.; Wattanathana, W.; Wannapaiboon, S.; Hanlumyuang, Y.; Sukthavorn, K.; Nootsuwan, N.; Chotiwan, S.; Phuthong, W.; Jongrungruangchok, S.; Laobuthee, A. Antimicrobial, Conductive, and Mechanical Properties of AgCB/PBS Composite System. *Journal of Chemistry* **2019**, *2019*, 1–14, doi:10.1155/2019/3487529.
23. Bin, T.; Qu, J.-P.; Liu, L.-M.; Feng, Y.-H.; Hu, S.-X.; Yin, X.-C. Non-isothermal crystallization kinetics and dynamic mechanical thermal properties of poly(butylene succinate) composites reinforced with cotton stalk bast fibers. *Thermochimica Acta* **2011**, *525*, 141–149, doi:10.1016/j.tca.2011.08.003.
24. Haghdan, S.; Smith, G. D. Natural fiber reinforced polyester composites: A literature review. *Journal of Reinforced Plastics and Composites* **2015**, *34*, 1179–1190, doi:10.1177/0731684415588938.
25. Mochane, M. J.; Magagula, S. I.; Sefadi, J. S.; Mokhena, T. C. A Review on Green Composites Based on Natural Fiber-Reinforced Polybutylene Succinate (PBS). *Polymers* **2021**, *13*, doi:10.3390/polym13081200.
26. Xiao, F.; Fontaine, G.; Bourbigot, S. Recent developments in fire retardancy of polybutylene succinate. *Polymer Degradation and Stability* **2021**, *183*, doi:10.1016/j.polymdegradstab.2020.109466.
27. Qasim, U.; Osman, A. I.; Al-Muhtaseb, A.a.H.; Farrell, C.; Al-Abri, M.; Ali, M.; Vo, D.-V. N.; Jamil, F.; Rooney, D. W. Renewable cellulosic nanocomposites for food packaging to avoid fossil fuel plastic pollution: a review. *Environmental Chemistry Letters* **2021**, *19*, 613–641, doi:10.1007/s10311-020-01090-x.
28. He, D.; Luo, Y.; Lu, S.; Liu, M.; Song, Y.; Lei, L. Microplastics in soils: Analytical methods, pollution characteristics and ecological risks. *TrAC Trends in Analytical Chemistry* **2018**, *109*, 163–172, doi:10.1016/j.trac.2018.10.006.
29. Karlsson, T. M.; Vethaak, A. D.; Almroth, B. C.; Ariese, F.; van Velzen, M.; Hassellöv, M.; Leslie, H. A. Screening for microplastics in sediment, water, marine invertebrates and fish: Method development and microplastic accumulation. *Marine Pollution Bulletin* **2017**, *122*, 403–408, doi:10.1016/j.marpolbul.2017.06.081.
30. Rudnik, E. 13 - Compostable Polymer Properties and Packaging Applications. In *Plastic Films in Food Packaging*, Ebnesajjad, S., Ed. William Andrew Publishing: Oxford, 2013, 217–248, doi:10.1016/B978-1-4557-3112-1.00013-2pp.

31. Jiang, L.; Zhang, J. 7 – Biodegradable and Biobased Polymers. In *Applied Plastics Engineering Handbook (Second Edition)*, Kutz, M., Ed. William Andrew Publishing: 2017, 127–143. doi:10.1016/B978-0-323-39040-8.00007-9pp.
32. BioPBS™. Availabe online: https://www.mcpp-global.com/en/asia/products/brand/biopbstm/ (accessed on 05.05.2021).
33. Brunner, C. T.; Baran, E. T.; Pinho, E. D.; Reis, R. L.; Neves, N.M. Performance of biodegradable microcapsules of poly(butylene succinate), poly(butylene succinate-co-adipate) and poly(butylene terephthalate-co-adipate) as drug encapsulation systems. *Colloids and Surfaces B: Biointerfaces* **2011**, *84*, 498–507, doi:10.1016/j.colsurfb.2011.02.005.
34. Sonseca, A.; Sahay, R.; Stepien, K.; Bukala, J.; Wcislek, A.; McClain, A.; Sobolewski, P.; Sui, X.; Puskas, J.E.; Kohn, J., et al. Architectured helically coiled scaffolds from elastomeric poly(butylene succinate) (PBS) copolyester via wet electrospinning. *Materials Science and Engineering: C* **2020**, *108*, 110505, doi:10.1016/j.msec.2019.110505.
35. Car interiors go green. Availabe online: https://www.plastics.gl/automotive/car-interiors-go-green/ (accessed on 05.05.2021).
36. Nikolic, M. S.; Djonlagic, J. Synthesis and characterization of biodegradablepoly(butylene succinate-co-butylene adipate)s. *Polymer Degradation and Stability* **2001**, *74*, 263–270, doi:10.1016/S0141-3910(01)00156-2.
37. Eichhorn, S.J.; Baillie, C.A.; Zafeiropoulos, N.; Mwaikambo, L.Y.; Ansell, M.P.; Dufresne, A.; Entwistle, K. M.; Herrera-Framco, P. J.; Escamilla, G. C.; Groom, L., et al. Review: current international research into cellulosic fibres and composites. *Journal of materials science* **2001**, *36*, 2107–2131, doi:10.1023/A:1017512029696.
38. Maksimov, R. D.; Gaidukovs, S.; Zicans, J.; Kalnins, M.; Plume, E.; Spacek, V.; Sviglerova, P. Nanocomposites based on a styrene-acrylate copolymer and organically modified montmorillonite 1. Mechanical properties. *Mechanics of Composite Materials* **2006**, *42*, 263–272, doi:10.1007/s11029-006-0036-1.
39. Gaidukov, S.; Danilenko, I.; Gaidukova, G. Characterization of strong and crystalline polyvinyl alcohol/montmorillonite films prepared by layer-by-layer deposition method. *International Journal of Polymer Science* **2015**, *2015*, doi:10.1155/2015/123469.
40. Gaidukovs, S.; Zukulis, E.; Bochkov, I.; Vaivodiss, R.; Gaidukova, G. Enhanced mechanical, conductivity, and dielectric characteristics of ethylene vinyl acetate copolymer composite filled with carbon nanotubes. *Journal of Thermoplastic Composite Materials* **2018**, *31*, 1161–1180, doi:10.1177/0892705717734603.
41. Graupner, N.; Ziegmann, G.; Wilde, F.; Beckmann, F.; Müssig, J. Procedural influences on compression and injection moulded cellulose fibre-reinforced polylactide (PLA) composites: Influence of fibre loading, fibre length, fibre orientation and voids. *Composites Part A: Applied Science and Manufacturing* **2016**, *81*, 158–171, doi:10.1016/j.compositesa.2015.10.040.
42. Fan, M.; Dai, D.; Huang, B. 3 Fourier Transform Infrared Spectroscopy for Natural Fibres. *Fourier Transform-Materials Analysis* **2012**, 10.5772/35482, doi:10.5772/35482.
43. Ciolacu, D.; Ciolacu, F.; Popa, V.I. Amorphous cellulose – structure and characterization. *Cellulose Chemistry and Technology* **2011**, *45*, 13–21.
44. Gowman, A.; Wang, T.; Rodriguez-Uribe, A.; Mohanty, A. K.; Misra, M. Bio-poly(butylene succinate) and Its Composites with Grape Pomace: Mechanical Performance and Thermal Properties. *ACS Omega* **2018**, *3*, 15205–15216, doi:10.1021/acsomega.8b01675.

45. Lin, N.; Yu, J.; Chang, P. R.; Li, J.; Huang, J. Poly(butylene succinate)-based biocomposites filled with polysaccharide nanocrystals: Structure and properties. *Polymer Composites* **2011**, *32*, 472–482, doi:10.1002/pc.21066.
46. Kim, H.-S.; Kim, H.-J.; Lee, J.-W.; Choi, I.-G. Biodegradability of bio-flour filled biodegradable poly(butylene succinate) bio-composites in natural and compost soil. *Polymer Degradation and Stability* **2006**, *91*, 1117–1127, doi:10.1016/j.polymdegradstab.2005.07.002.
47. Kruer-Zerhusen, N.; Cantero-Tubilla, B.; Wilson, D. B. Characterization of cellulose crystallinity after enzymatic treatment using Fourier transform infrared spectroscopy (FTIR). *Cellulose* **2017**, *25*, 37–48, doi:10.1007/s10570-017-1542-0.
48. Dong, C.; Takagi, H. Flexural properties of cellulose nanofibre reinforced green composites. *Composites Part B: Engineering* **2014**, *58*, 418–421, doi:10.1016/j.compositesb.2013.10.032.
49. Frollini, E.; Bartolucci, N.; Sisti, L.; Celli, A. Poly(butylene succinate) reinforced with different lignocellulosic fibers. *Industrial Crops and Products* **2013**, *45*, 160–169, doi:10.1016/j.indcrop.2012.12.013.
50. Xu, J.; Manepalli, P.H.; Zhu, L.; Narayan-Sarathy, S.; Alavi, S. Morphological, barrier and mechanical properties of films from poly (butylene succinate) reinforced with nanocrystalline cellulose and chitin whiskers using melt extrusion. *Journal of Polymer Research* **2019**, *26*, doi:10.1007/s10965-019-1783-8.
51. Kuan, C. F.; Ma, C. C. M.; Kuan, H. C.; Wu, H. L.; Liao, Y. M. Preparation and characterization of the novel water-crosslinked cellulose reinforced poly(butylene succinate) composites. *Composites Science and Technology* **2006**, *66*, 2231–2241, doi:10.1016/j.compscitech.2005.12.011.
52. Kowalczyk, M.; Piorkowska, E.; Kulpinski, P.; Pracella, M. Mechanical and thermal properties of PLA composites with cellulose nanofibers and standard size fibers. *Composites Part A: Applied Science and Manufacturing* **2011**, *42*, 1509–1514, doi:10.1016/j.compositesa.2011.07.003.
53. Crean, A. Evaluation of Various Brands of Moisture Meters in Gypsum and Wood Substrates at a Range of Moisture Contents. *Civil Engineering Journal* **2017**, *3*, 640–649, doi:10.21859/cej-03091.
54. Kuka, E.; Cirule, D.; Kajaks, J.; Andersone, I.; Andersons, B. Wood particle size influence on water resistance and mechanical properties of thermally modified wood-polypropylene composites. *International Wood Products Journal* **2018**, *9*, 90–95, doi:10.1080/20426445.2018.1493069.
55. Bhasney, S. M.; Bhagabati, P.; Kumar, A.; Katiyar, V. Morphology and crystalline characteristics of polylactic acid [PLA]/linear low density polyethylene [LLDPE]/microcrystalline cellulose [MCC] fiber composite. *Composites Science and Technology* **2019**, *171*, 54–61, doi:10.1016/j.compscitech.2018.11.028.
56. Shi, K.; Liu, Y.; Hu, X.; Su, T.; Li, P.; Wang, Z. Preparation, characterization, and biodegradation of poly(butylene succinate)/cellulose triacetate blends. *International Journal of Biological Macromolecules* **2018**, *114*, 373–380, doi:10.1016/j.ijbiomac.2018.03.151.
57. Lizundia, E.; Vilas, J. L.; León, L. M. Crystallization, structural relaxation and thermal degradation in Poly(l-lactide)/cellulose nanocrystal renewable nanocomposites. *Carbohydrate Polymers* **2015**, *123*, 256–265, doi:10.1016/j.carbpol.2015.01.054.
58. Shen, D. K.; Gu, S. The mechanism for thermal decomposition of cellulose and its main products. *Bioresource Technology* **2009**, *100*, 6496–6504, doi:10.1016/j.biortech.2009.06.095.

59. Chrissafis, K.; Paraskevopoulos, K. M.; Bikiaris, D. N. Thermal degradation mechanism of poly(ethylene succinate) and poly(butylene succinate): Comparative study. *Thermochimica Acta* **2005**, *435*, 142–150, doi:10.1016/j.tca.2005.05.011.
60. *Green biorenewable biocomposites from knowledge to industrial applications*. 1st Edition ed.; Thakur, V. K.; Kessler, M. R., Eds.; Apple Academic Press New York, 2015, doi:10.1201/b18092p 568.
61. Das, S. Mechanical and water swelling properties of waste paper reinforced unsaturated polyester composites. *Construction and Building Materials* **2017**, *138*, 469–478, doi:10.1016/j.conbuildmat.2017.02.041.
62. Fortunati, E.; Rinaldi, S.; Peltzer, M.; Bloise, N.; Visai, L.; Armentano, I.; Jiménez, A.; Latterini, L.; Kenny, J. M. Nano-biocomposite films with modified cellulose nanocrystals and synthesized silver nanoparticles. *Carbohydrate Polymers* **2014**, *101*, 1122–1133, doi:10.1016/j.carbpol.2013.10.055.
63. Kim, H. S.; Kim, H. J.; Lee, J. W.; Choi, I. G. Biodegradability of bio-flour filled biodegradable poly(butylene succinate) bio-composites in natural and compost soil. *Polymer Degradation and Stability* **2006**, *91*, 1117–1127, doi:10.1016/j.polymdegradstab.2005.07.002.
64. Luzi, F.; Fortunati, E.; Jiménez, A.; Puglia, D.; Pezzolla, D.; Gigliotti, G.; Kenny, J. M.; Chiralt, A.; Torre, L. Production and characterization of PLA_PBS biodegradable blends reinforced with cellulose nanocrystals extracted from hemp fibres. *Industrial Crops and Products* **2016**, *93*, 276–289, doi:10.1016/j.indcrop.2016.01.045.
65. Huang, F.-Y. Thermal Properties and Thermal Degradation of Cellulose Tri-Stearate (CTs). *Polymers* **2012**, *4*, 1012–1024, doi:10.3390/polym4021012.
66. Yuwawech, K.; Wootthikanokkhan, J.; Tanpichai, S. Effects of Two Different Cellulose Nanofiber Types on Properties of Poly(vinyl alcohol) Composite Films. *Journal of Nanomaterials* **2015**, *2015*, 1–10, doi:10.1155/2015/908689.
67. Tan, V.; Abdallah, W.; Kamal, M.R. The Effect of Cellulose Nanocrystals (CNC) on Isothermal Crystallization Kinetics of LLDPE and HDPE. *International Polymer Processing* **2018**, *33*, 371–380, doi:10.3139/217.3559.
68. Dufresne, A.; Kellerhals, M. B.; Witholt, B. Transcrystallization in Mcl-PHAs/cellulose whiskers composites. *Macromolecules* **1999**, *32*, 7396–7401, doi:10.1021/ma990564r.
69. Qi, X.; Yang, G.; Jing, M.; Fu, Q.; Chiu, F.-C. Microfibrillated cellulose-reinforced bio-based poly(propylene carbonate) with dual shape memory and self-healing properties. *Journal of Materials Chemistry A* **2014**, *2*, 20393–20401, doi:10.1039/c4ta04954c.
70. Boparai, K. S.; Singh, R. Thermoplastic Composites for Fused Deposition Modeling Filament: Challenges and Applications. In *Reference Module in Materials Science and Materials Engineering*, Elsevier: 2018, doi:10.1016/B978-0-12-803581-8.11409-2.
71. Mathew, A. P.; Oksman, K.; Sain, M. Mechanical properties of biodegradable composites from poly lactic acid (PLA) and microcrystalline cellulose (MCC). *Journal of Applied Polymer Science* **2005**, *97*, 2014–2025, doi:10.1002/app.21779.
72. Ferreira, F. V.; Pinheiro, I. F.; Mariano, M.; Cividanes, L. S.; Costa, J. C. M.; Nascimento, N. R.; Kimura, S. P. R.; Neto, J. C. M.; Lona, L. M. F. Environmentally friendly polymer composites based on PBAT reinforced with natural fibers from the amazon forest. *Polymer Composites* **2019**, *40*, 3351–3360, doi:10.1002/pc.25196.
73. Ferreira, F.; Pinheiro, I.; de Souza, S.; Mei, L.; Lona, L. Polymer Composites Reinforced with Natural Fibers and Nanocellulose in the Automotive Industry: A Short Review. *Journal of Composites Science* **2019**, *3*, doi:10.3390/jcs3020051.
74. Siqueira, G.; Bras, J.; Follain, N.; Belbekhouche, S.; Marais, S.; Dufresne, A. Thermal and mechanical properties of bio-nanocomposites reinforced by Luffa cylindrica

cellulose nanocrystals. *Carbohydrate Polymers* **2013**, *91*, 711–717, doi:10.1016/j.carbpol.2012.08.057.
75. Tanpichai, S.; Quero, F.; Nogi, M.; Yano, H.; Young, R. J.; Lindstrom, T.; Sampson, W. W.; Eichhorn, S. J. Effective Young's modulus of bacterial and microfibrillated cellulose fibrils in fibrous networks. *Biomacromolecules* **2012**, *13*, 1340–1349, doi:10.1021/bm300042t.
76. Ichazo, M. N.; Albano, C.; Gonzalez, J.; Perera, R.; Candal, M. V. Polypropylene/wood flour composites: treatments and properties. *Composite Structures* **2001**, *54*, 207–214, doi:10.1016/S0263-8223(01)00089-7.
77. Liang, Z.; Pan, P.; Zhu, B.; Dong, T.; Inoue, Y. Mechanical and thermal properties of poly(butylene succinate)/plant fiber biodegradable composite. *Journal of Applied Polymer Science* **2010**, *115*, 3559–3567, doi:10.1002/app.29848.
78. Hee-Soo, K.; Han-Seung, Y.; Hyun-Joong, K. Biodegradability and mechanical properties of agro-flour-filled polybutylene succinate biocomposites. *Journal of Applied Polymer Science* **2005**, *97*, 1513–1521, doi:10.1002/app.21905.
79. Kajaks, J.; Kalnins, K.; Naburgs, R. Wood plastic composites (WPC) based on high-density polyethylene and birch wood plywood production residues. *International Wood Products Journal* **2017**, *9*, 15–21, doi:10.1080/20426445.2017.1410997.
80. Mizuno, S.; Maeda, T.; Kanemura, C.; Hotta, A. Biodegradability, reprocessability, and mechanical properties of polybutylene succinate (PBS) photografted by hydrophilic or hydrophobic membranes. *Polymer Degradation and Stability* **2015**, *117*, 58–65, doi:10.1016/j.polymdegradstab.2015.03.015.
81. Sakai, Y.; Isokawa, M.; Masuda, T.; Yoshioka, H.; Hayastsu, M.; Hayono, K. Usefulness of Soil p-Nitrophenyl Acetate Esterase Activity as a Tool to Monitor Biodegradation of Polybutylene Succinate (PBS) in Cultivated Soil. *Polymer Journal* **2002**, *34*, 767–774, doi:10.1295/polymj.34.767.
82. Hee-Soo, K.; Hyun-Joong, K.; Jae-Won, L.; In-Gyu, C. Biodegradability of bio-flour filled biodegradable poly(butylene succinate) bio-composites in natural and compost soil. *Polymer Degradation and Stability* **2006**, *91*, 1117–1127, doi:10.1016/j.polymdegradstab.2005.07.002.
83. Hu, X.; Su, T.; Pan, W.; Li, P.; Wang, Z. Difference in solid-state properties and enzymatic degradation of three kinds of poly(butylene succinate)/cellulose blends. *RSC Advances* **2017**, *7*, 35496–35503, doi:10.1039/c7ra04972b.
84. Josefsson, G.; Berthold, F.; Gamstedt, E. K. Stiffness contribution of cellulose nanofibrils to composite materials. *International Journal of Solids and Structures* **2014**, *51*, 945–953, doi:10.1016/j.ijsolstr.2013.11.018.
85. Rastogi, V. K.; Samyn, P. Novel processing of polyhydroxybutyrate with micro- to nanofibrillated cellulose and effect of fiber morphology on crystallization behaviour of composites. *Express Polymer Letters* **2020**, *14*, 115–133, doi:10.3144/expresspolymlett.2020.11.
86. Lv, Z.-Y.; Zhang, M. C.; Zhang, Y.; Guo, B.-H.; Xu, J. Study on melting and recrystallization of poly(butylene succinate) lamellar crystals via step heating differential scanning calorimetry. *Chinese Journal of Polymer Science* **2017**, *35*, 1552–1560, doi:10.1007/s10118-017-1986-6.
87. Zaaba, N. F.; Jaafar, M.; Ismail, H. Tensile and morphological properties of nanocrystalline cellulose and nanofibrillated cellulose reinforced PLA bionanocomposites: A review. *Polymer Engineering & Science* **2020**, doi:10.1002/pen.25560.

88. Gan, P. G.; Sam, S. T.; Abdullah, M. F. B.; Omar, M. F. Thermal properties of nanocellulose-reinforced composites: A review. *Journal of Applied Polymer Science* **2019**, *137*, doi:10.1002/app.48544.
89. Li, Y. D.; Fu, Q. Q.; Wang, M.; Zeng, J. B. Morphology, crystallization and rheological behavior in poly(butylene succinate)/cellulose nanocrystal nanocomposites fabricated by solution coagulation. *Carbohydrate Polymers* **2017**, *164*, 75–82, doi:10.1016/j.carbpol.2017.01.089.
90. Wang, T.; Drzal, L. T. Cellulose-nanofiber-reinforced poly(lactic acid) composites prepared by a water-based approach. *ACS Applied Materials & Interfaces* **2012**, *4*, 5079–5085, doi:10.1021/am301438g.
91. Xu, X.; Liu, F.; Jiang, L.; Zhu, J. Y.; Haagenson, D.; Wiesenborn, D. P. Cellulose nanocrystals vs. cellulose nanofibrils: a comparative study on their microstructures and effects as polymer reinforcing agents. *ACS Applied Materials & Interfaces* **2013**, *5*, 2999–3009, doi:10.1021/am302624t.
92. Cailloux, J.; Raquez, J. M.; Lo Re, G.; Santana, O.; Bonnaud, L.; Dubois, P.; Maspoch, M. L. Melt-processing of cellulose nanofibril/polylactide bionanocomposites via a sustainable polyethylene glycol-based carrier system. *Carbohydrate Polymers* **2019**, *224*, 115188, doi:10.1016/j.carbpol.2019.115188.
93. Chen, R.-Y.; Zou, W.; Zhang, H.-C.; Zhang, G.-Z.; Yang, Z.-T.; Jin, G.; Qu, J.-P. Thermal behavior, dynamic mechanical properties and rheological properties of poly(butylene succinate) composites filled with nanometer calcium carbonate. *Polymer Testing* **2015**, *42*, 160–167, doi:10.1016/j.polymertesting.2015.01.015.
94. Platnieks, O.; Gaidukovs, S.; Barkane, A.; Gaidukova, G.; Grase, L.; Thakur, V. K.; Filipova, I.; Fridrihsone, V.; Skute, M.; Laka, M. Highly Loaded Cellulose/Poly (butylene succinate) Sustainable Composites for Woody-Like Advanced Materials Application. *Molecules* **2019**, *25*, doi:10.3390/molecules25010121.
95. Platnieks, O.; Barkane, A.; Ijudina, N.; Gaidukova, G.; Thakur, V. K.; Gaidukovs, S. Sustainable tetra pak recycled cellulose / Poly(Butylene succinate) based woody-like composites for a circular economy. *Journal of Cleaner Production* **2020**, *270*, 122321, doi:10.1016/j.jclepro.2020.122321.
96. Eubeler, J. P.; Bernhard, M.; Knepper, T. P. Environmental biodegradation of synthetic polymers II. Biodegradation of different polymer groups. *TrAC – Trends in Analytical Chemistry* **2010**, *29*, 84–100, doi:10.1016/j.trac.2009.09.005.
97. Shah, A. A.; Kato, S.; Shintani, N.; Kamini, N. R.; Nakajima-Kambe, T. Microbial degradation of aliphatic and aliphatic-aromatic co-polyesters. *Applied Microbiology and Biotechnology* **2014**, *98*, 3437–3447, doi:10.1007/s00253-014-5558-1.
98. Kim, H. S.; Kim, H. J. Enhanced hydrolysis resistance of biodegradable polymers and bio-composites. *Polymer Degradation and Stability* **2008**, *93*, 1544–1553, doi:10.1016/j.polymdegradstab.2008.05.004.

Oskars Platnieks received a Master's degree in Materials Science from Riga Technical University (RTU) in 2017. His field of research is bio-based and naturally degradable materials. He has been studying these materials since his master's studies. His Tesis research was carried out at the RTU Institute of Polymer Materials, where he pursues active research. His research goal is to address sustainability issues and adapt them to the requirements of modern polymer and composite materials.